
CORESPECT: ENHANCING CLUSTERING ALGORITHMS VIA AN INTERPLAY OF DENSITY AND GEOMETRY

Chandra Sekhar Mukherjee^{*†}, Joonyoung Bae^{*‡}, Jiapeng Zhang[§]

Thomas Lord Department of Computer Science
University of Southern California

July 14, 2025

ABSTRACT

Density and geometry have long served as two of the fundamental guiding principles in clustering algorithm design, with algorithm usually focusing either on the density structure of the data (e.g., HDBSCAN and Density Peak Clustering) or the complexity of underlying geometry (e.g., manifold clustering algorithms).

In this paper, we identify and formalize a recurring but often overlooked interaction between distribution and geometry and leverage this insight to design our clustering enhancement framework **CoreSPECT (Core Space Projection-based Enhancement of Clustering Techniques)**. Our framework boosts the performance of simple algorithms like K-Means and GMM by applying them to strategically selected regions, then extending the partial partition to a complete partition for the dataset using a novel neighborhood graph based multi-layer propagation procedure.

We apply our framework on **15 datasets from three different domains** and obtain consistent and substantial gain in clustering accuracy for both K-Means and GMM. On average, our framework improves the ARI of K-Means by **40%** and of GMM by **14%**, often surpassing the performance of both manifold-based and recent density-based clustering algorithms. We further support our framework with initial theoretical guarantees, ablation to demonstrate the usefulness of the individual steps and with evidence of robustness to noise.

1 Introduction

Clustering is one of the most fundamental and well studied problems in the machine learning literature, having important applications in various domains such as cell type discovery in various biological data [SVY⁺18, HSL⁺23, LRSH⁺24], image classification [SM00, VL07], and others. Here, we are given a d -dimensional dataset X consisting of n points $\mathbf{x}_1, \dots, \mathbf{x}_n$ that has a (hidden) ground truth partition into some k clusters, represented as $V := \cup_{i=1}^k V_i$. The goal is to obtain a partition that is close to the ground truth.

As with any unsupervised learning algorithm, recovering the ground truth clusters of an arbitrary dataset is information theoretically impossible. Therefore, often algorithms aim to exploit the underlying structure w.r.t. the ground truth clusters. Design of clustering algorithms based on interpretable and effective assumptions has been a central area of research over the last 50 years.

The core assumptions behind clustering algorithms typically involve *some notion of separability* between the underlying clusters. As a starting point, we recall the well-known K-Means objective [Llo82]. When ground truth clusters are well-separated in the original embedding space and are sufficiently spherical, fast algorithms like K-Means++ [AV06]

^{*}Equal contribution.

[†]chandrasedkhar.mukherjee07@gmail.com

[‡]joonyoungbae.aaron@gmail.com

[§]jiapengz@usc.edu

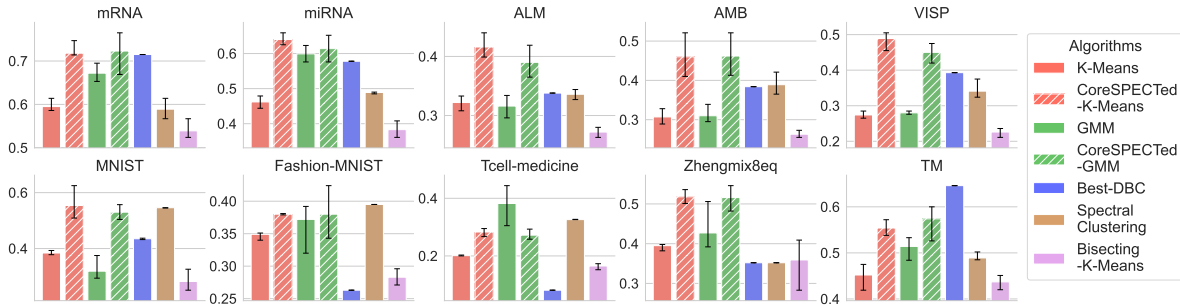


Figure 1: ARI of CoreSPECTed-K-Means and CoreSPECTed-GMM compared to that of K-Means and GMM, as well as Bisecting-K-Means, Spectral Clustering, and dataset-wise Best Density Based Clustering (Best-DBC) algorithms on 10 datasets from 3 domains.

can yield a partition close to ground truth. However, as the notion of separation becomes more complex, its performance degrades significantly. To deal with this scenario, clustering algorithms have increasingly focused on two aspects of the underlying structure, namely density and geometry.

Assumptions on density and geometry. Several algorithms are designed with assumptions about the density of the data. The usual assumption is that clusters have high density regions that are well separable with lower density regions between them. This notion has led to influential clustering algorithms like HDBSCAN [CMS13] and GMM [DLR77, YLL12] as well as the popular various Density Peak Clustering (DPC) algorithms [RL14, WX17, YEHS23].

Another line of research has focused on exploiting the underlying shape in the data. For instance, different clusters may lie on distinct regions of a low-dimensional manifold—or even on separate manifolds—despite appearing close in the original embedding space. Here, using local neighborhood based approximation of distances have led to several clustering algorithms [THL23, LMM20, VL07].

Contrasting with the typical focus on either the density or geometry of data, we observe that in many datasets, the geometric notion of cluster separability is closely correlated with the underlying density. This insight motivates the following contributions.

1.1 Contribution

1. **Modeling:** We observe that in many datasets, ground truth clusters contain dense regions that are well separated in the original embedding space, whereas the sparser regions are more nonlinear, while exhibiting a local notion of separability characterized by its proximity to these dense regions.

2. **Algorithm design:** Using these insights, we design a generic *4-step clustering enhancement framework* that improves the performance of simple geometric algorithms like K-Means and density-based algorithms like GMM on data with aforementioned structure. We provide statistical evidence that further support our model assumptions and initial theoretical support for several key components.

3. **Experiments:** We evaluate the improvements due to our framework for K-Means and GMM on 15 datasets (2 bulk RNA seq dataset, 2 image datasets, and 11 single-cell RNA seq datasets). On average, our framework improves ARI of K-Means by 40% and that of GMM by 14%. We show the comparative performance of 10 datasets in Figure 1. We also get substantial gains in NMI. In doing so, the improved K-Means and GMM often outperform sophisticated geometry-based algorithms like Spectral Clustering and density-based algorithms like HDBSCAN and recent DPC algorithms. Furthermore, we show that our framework is robust to noise in Section 4.3.

A high level description of our approach. We exploit three key properties in relation to the density-geometry correlation to build our clustering enhancement framework.

i) First, we observe that each ground truth cluster has a dense region (that we call *core*), such that these regions are separated enough for simple algorithms like greedy K-Means algorithm to partition.

ii) Next, we observe that as one moves away from these cores, two phenomena occur simultaneously. The density decreases, *and* the support of the points become *increasingly non-linear* w.r.t. the ground truth clusters, degrading the performance of simple algorithms like K-Means and GMM.

iii) However, we find that these points can be correctly clustered by considering the proximity of sparse points to *globally decided* denser regions in a layered manner, i.e., a sparse point’s proximity to high-density regions (rather than to other sparse points) more reliably indicates its cluster identity.

Our clustering enhancement framework is designed to systematically exploit these observations, as described in Section 2.1. We summarize the steps of the algorithm in Figure 3 and provide a schematic description in Figure 2. Essentially, our algorithm uses a clustering of the cores to achieve a better clustering of the whole data, where, the cluster-identity of each non-core point is expressed as a combination of the cluster-identity of the core points (in a layer-wise manner). This leads us to the name of **Core Space Projection**. We believe this idea can have applications beyond clustering, and is one of the exciting future directions.

1.2 Related works

Multi-core-periphery structure on graphs: In [MZ25], the authors observed that in the K-NN graph embedding of biological datasets with clustering structure, nodes with high centrality scores are more separable. They proposed the “multi-core-periphery with communities” structure and designed ranking algorithms based on relative centrality to detect the cores of all clusters—an idea that inspires part of our framework. However, their work has two limitations. Firstly, they leave open the question of how the graph structure translates back to the original feature space. Secondly, they do not propose any mechanism to leverage this structure for clustering the full dataset. In contrast, we observe a geometry-density correlation in data (described in Section 1.1) and use it to build a clustering enhancement framework that consistently improves clustering performance across diverse datasets.

Density and geometry based algorithms: Our framework leverages both geometric and density structures of data. We identify dense regions that are well-separated, while the surrounding outer layers exhibit more non-linear structure. In contrast, manifold clustering algorithms [VL07, LMM20, THL23] assume entire clusters lie on low-dimensional manifolds with complex Euclidean geometry, that leads to mechanisms with higher computation cost. Instead, we construct a density-guided graph to cluster these outer regions. This approach is inspired by DPC, which links each point to a higher-density neighbor to form a single-linkage structure, later pruned to extract clusters. However, DPC is sensitive to noise, and its pruning heuristics fail on complex geometries, as we observe.

Our framework enhances K-Means on datasets like MNIST and Fashion-MNIST—known to lie on non-linear low-dimensional manifolds [BTS⁺21]—making it competitive with Spectral Clustering, and outperforming it on several biological datasets (Figure 2). We also improve K-Means and GMM beyond state-of-the-art DPC variants, achieving significantly better robustness to noise (Figure 7).

Outline. In Section 2, we formally describe our model and framework, providing initial statistical and theoretical guarantees. Section 3 provides further statistical evidence supporting our assumption on the underlying model of the data. Section 4 contains large scale experiments on real-world datasets and comparison of performance with both density-based and manifold-based clustering algorithms, where we show that our framework enhances the performance of simple algorithms like K-Means beyond that of both kinds of algorithms. Then Section 5 further explores the importance and effect of each of our steps and the innovations therein. We conclude in Section 6 with discussion on limitations and future steps.

2 Model formulation and the CoreSPECT framework

In this Section we define our model assumptions on a high level. We require certain technical assumptions to prove our initial theoretical guarantees, which are presented in detail in Section A, along with all the proofs.

We assume points of each ground-truth cluster i is being generated from some $\mathcal{X}_i \subseteq \mathbb{R}^d$, where all the points lie on some m -dimensional smooth manifold \mathcal{M} . We make the following assumptions on the geometry-density interaction.

Concentric subspaces The fundamental assumption we make is that \mathcal{X}_i can be expressed as a hierarchy of concentric subspaces $\mathcal{X}_{i,0} \subset \mathcal{X}_{i,1} \subset \dots \subset \mathcal{X}_{i,\ell-2} \subset \mathcal{X}_{i,\ell-1} = \mathcal{X}_i$. We call the difference between the j and $j+1$ -th subspace as the j -th layer $\mathcal{L}_{i,j}$, defined as

$$\mathcal{L}_{i,0} := \mathcal{X}_{i,0}, \quad \mathcal{L}_{i,j} := \mathcal{X}_{i,j} \setminus \mathcal{X}_{i,j-1}, \quad 1 \leq j < \ell$$

Here we assume that each $\mathcal{L}_{i,j}$ are smooth and have a minimum and maximum depth in any direction. We call the $\mathcal{L}_{i,0}$ as *cores* and the outer layers as more peripheral. We assume each layer is connected and has finite volume in a well-defined measure. We make the following assumptions, that we collectively term as the Layered-core-periphery-density-model (LCPDM).

The Layered-core-periphery-density-model LCPDM(k, ℓ):

1. *Cores are dense and peripheries are sparse:* The data is generated by sampling $n_{i,j}$ points from each layer $\mathcal{L}_{i,j}$ uniformly at random, such that there exists a constant $C > 1$ satisfying

$$\frac{n_{i,j}}{\text{Vol}(\mathcal{L}_{i,j})} > C \cdot \frac{n_{i,j+1}}{\text{Vol}(\mathcal{L}_{i,j+1})}$$

That is, for each cluster, the inner-most layer (the core) is the densest, and the density of the outer layer monotonically go down. We present this schematically in Figure 2 (a). We denote the points generated from $\mathcal{L}_{i,j}$ as $\hat{\mathcal{L}}_{i,j}$.

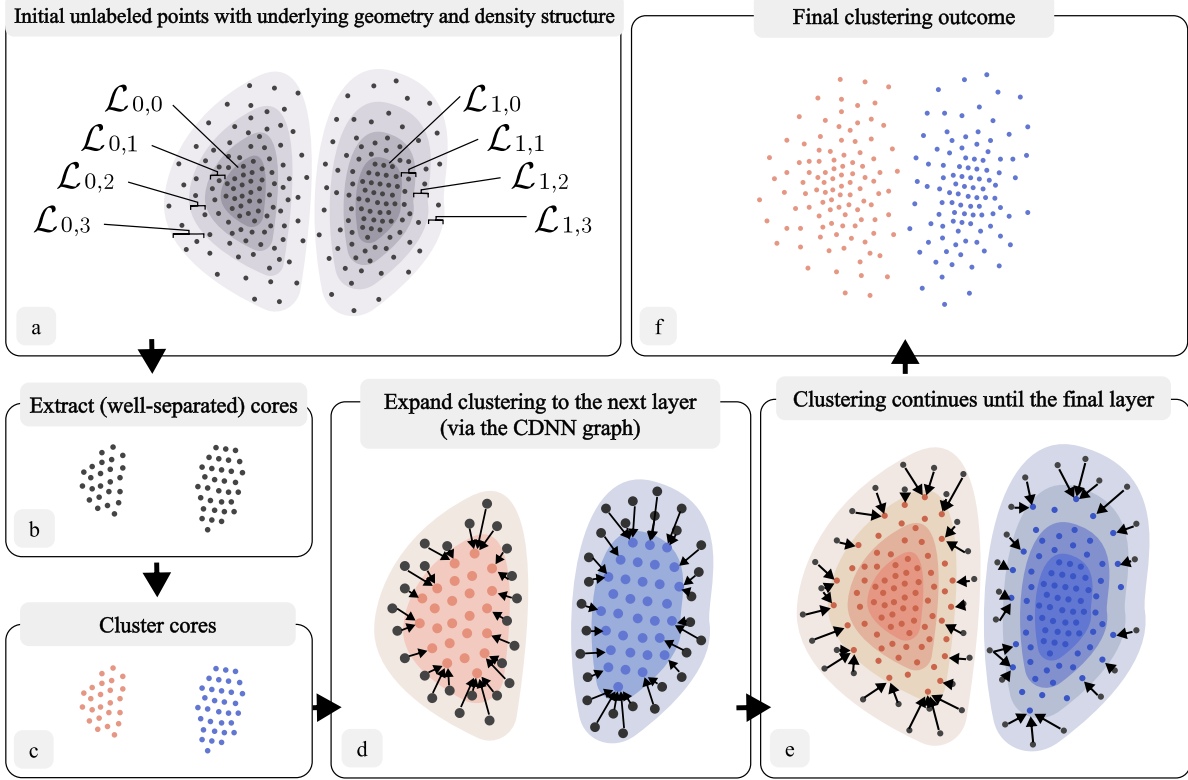


Figure 2: The underlying geometry-density structure in the data (a), and the step-by-step execution of the CoreSPECT framework. In step (b) we extract the cores. Then, in step (c) we cluster the cores with a simple algorithm. Steps (d) \rightarrow (f) exhibit the layer-wise expansion of clustering using the CDNN graph.

2. *Cores are well-separated.* The first assumption on the geometry dictates that the core-layers of the clusters are well separated in an Euclidean sense. For any clusters i, i'

$$\exists \mu_{i,i'} < 0.5 \quad \text{s.t.} \quad \max_{\mathbf{x} \in \hat{\mathcal{L}}_{i,0}, \mathbf{x}' \in \hat{\mathcal{L}}_{i',0}} \|\mathbf{x} - \mathbf{x}'\| \leq \mu_{i,i'} \cdot \min_{\mathbf{x} \in \hat{\mathcal{L}}_{i,0}, \mathbf{x}' \in \hat{\mathcal{L}}_{i',0}} \|\mathbf{x} - \mathbf{x}'\|$$

When there are only two clusters in the data, we define $\mu := \mu_{0,1}$.

3. *Layer-wise clustering membership alignment.* There exists $\delta < 1$ such that for any $\mathbf{x} \in \mathcal{L}_{i,j}$ and any $i' \neq i$, $\min_{\mathbf{x}' \in \mathcal{L}_{i',j-1}} \|\mathbf{x} - \mathbf{x}'\| \leq \delta \cdot \min_{\mathbf{x}'' \in \mathcal{L}_{i',j-1}} \|\mathbf{x} - \mathbf{x}''\|$.

That is, any point in a cluster is closer to the boundary of the inner-layer of the same cluster than points in inner-layer of another cluster. Additionally, we do not make any assumptions on the geometry and proximity of points in the outermost layers.

2.1 The CoreSPECT framework

We first give a brief outline of our framework in Figure 3. We stress that the specific algorithms for each of the step in our framework can be further improved as long as they satisfy certain properties that we describe. For demonstration of the framework, we will use two hard-to-separate clusters (0,2) of the popular Fashion-MNIST dataset for which K-Means has a poor performance. We make certain curvature assumptions on the inner layer (but not the outer-most layer) for proving our theorems that we explain in detail in the supplementary material.

2.1.1 Step 1: Extracting the cores (and the subsequent layers)

We first recover the density layers, estimating the core $\hat{\mathcal{L}}_0$ with S_0 that is well-separated in an Euclidean sense, and also the subsequent layers.

1. **Step 1: Core (and subsequent density layers) extraction (Figure 2 (a), (b)).** We have described in our model that each cluster has some ℓ layers $\mathcal{L}_{i,j}, 0 \leq j \leq \ell - 1$. We first want to obtain $\hat{\mathcal{L}}_0 := \cup_{i=1}^k \hat{\mathcal{L}}_{i,0}$, that is, approximately the union of cores of all the clusters. Crucially, we do this *without* any clustering, but rather exploiting the density structure in the hierarchies. We describe this step in Section 2.1.1. We extend this to get an estimate of union of the outer density layers $\hat{\mathcal{L}}_j, 1 \leq j < \ell$. **We use S_j to denote our estimate of $\hat{\mathcal{L}}_j$.**
2. **Step 2: Clustering the core (Figure 2 (c)).** In this step, the cores (S_0) are clustered with a simple algorithm of user’s choice. In our explanations and dry run, we use K-Means. We describe the rationale behind this in Section 2.1.2.
3. **Step 3: Core directed nearest neighbor (CDNN) graph construction (Figure 2 (d)).** Next, we design a novel layer-by-layer nearest neighbor graph structure using the estimated density layers S_j and show that it captures the underlying cluster structure of the data better than Euclidean distance. This is described in Section 2.1.3.
4. **Step 4: Layer-wise expansion of clustering (Figure 2 (d)→(f)).** Finally, we use the clustering of the core obtained in Step 2 and the graph in Step 3 to cluster each of the layers in the hierarchy in time *Linear in the number of points, clusters, and nearest neighbors to check*. This is described in Section 2.1.4.

Figure 3: The CoreSPECT Framework (See Figure 2 for a schematic representation and Algorithm 4 for its application to K-Means)

Definition 1 (Layer-preserving ranking). *Given a dataset X generated from the LCPDM(k, ℓ) model, we say a ranking of the points in X is layer-preserving if for any cluster \mathcal{X}_i , if $\mathbf{x} \in \hat{\mathcal{L}}_{i,j}$ and $\mathbf{x}' \in \hat{\mathcal{L}}_{i,j'}$, where $j < j'$, then \mathbf{x} is ranked above \mathbf{x}' .*

Our ranking algorithm is motivated by the *relative centrality framework* of [MZ25], designed to obtain the central parts of *each community*. In contrast, we aim to find the *densest regions of each cluster*. In this direction, we obtain a q-NN graph $G_{q,X}$ and obtain the distribution of $\log(n)$ step random walk, denoted as $\Pi(G_{q,X})$, mimicking *initial centrality* of [MZ25]. However, we note (and explore in the appendix) that their notion of relative centrality does not capture the density hierarchies in the underlying data. To circumvent this, we define the concept of *relative density*.

Relative density estimation. Given a dataset X with density estimation $P : V \rightarrow [0, 1]$ for each data point, we look at its r -nearest neighbors, and randomly move to one of the neighbors that have a higher P value, continuing the process until we reach a maxima, as described in Algorithm 1.

Then, our core-ranking algorithm, *FlowRank* (Algorithm 2) calculates the average between the density of a point, and that of the average maxima reached by randomly ascending random walks starting from that point. We provide the following guarantee for the ranking, with the proof (and the proofs of the following theorems) pushed to the supplementary material.

Algorithm 1 RARW(X, Π, r, i)
(Randomly Ascending Random Walk)

Input: $X, \Pi : X \rightarrow [0, 1]$ and index i .
Let $N_r(\mathbf{x})$ be the r closest points to \mathbf{x} .
Start: $\mathbf{x}^+ \leftarrow \mathbf{x}_i$
while $\Pi(\mathbf{x}^+) < \max_{\mathbf{x}' \in N_r(\mathbf{x}^+)} \Pi(\mathbf{x}')$ **do**
 $N^+ \leftarrow \mathbf{x}' \in N_r(\mathbf{x}^+) : \Pi(\mathbf{x}') > \Pi(\mathbf{x}^+)$
 Randomly select a point \mathbf{x}'' from N^+
 $\mathbf{x}^+ \leftarrow \mathbf{x}''$
end while
return $\Pi(\mathbf{x}^+)$

Algorithm 2 FlowRank: FR(X, Π, q, r)

Input: X , a $n \times d$ dataset, neighborhood parameter r , density vector Π .

(We obtain the density estimation through a $\log n$ -step random walk simulation on $G_{q,X}$.)

for i in $1:n$ **do**
 $z_i \leftarrow \mathbb{E}[\text{RARW}(X, \Pi, r, i)]$
 $score[i] \leftarrow \frac{\Pi_i}{z_i}$
end for

Theorem 1 (Core-detection by FlowRank). *Let data be generated from the LCPDM($2, \ell$) model, with a chosen $r = \mathcal{O}(1)$. Assume we get the exact density of the points and expected value of randomly ascending random walk in the FlowRank algorithm. In such a case all the core points ($\hat{\mathcal{L}}_0$) get a score of 1. Additionally, all non-core points get a score < 1 .*

In practice, we observe selecting top 10% ranked points as the core works well, as it consists of points from each underlying cluster and we will observe the top-points are also very separable. Additionally, we define the next 10% blocks as our proxy for the layers $\hat{\mathcal{L}}_j$. Here we note that in different datasets, the number of layers may vary, however, if the ranking is layer preserving, our partition either breaks a single layer into multiple ones, or only merges multiple *consecutive* layers into one. Obtaining a better approximation of $\hat{\mathcal{L}}_j$ is a primary direction towards improving our framework.

Observation (Fashion-MNIST $\{0, 2\}$: Core extraction). *The top 10% ranked points obtained by FlowRank contain an almost equal number of points from each cluster.*

2.1.2 Step 2: Applying the clustering algorithm to the core

Here, we formally (as well as experimentally) capture the separability of the cores by K-Means.

Proposition 1. *Let n_0 and n_1 points ($n_0 > n_1$ WLOG) be sampled from $\mathcal{X}_{0,0}$ and $\mathcal{X}_{1,0}$ respectively such that $\mu \cdot n_0 \leq n_1$. These points are denoted $\hat{\mathcal{L}}_{0,0}$ and $\hat{\mathcal{L}}_{1,0}$. Consider the slightly modified K-Means algorithm. Obtain two centers using the K-Means++ method and run one-step K-Means. Repeat this process some $2 \log n$ times and accept the result with minimum K-Means objective value. This algorithm separates the two cores correctly with probability $1 - o(1)$.*

Observation (Fashion-MNIST $\{0, 2\}$: K-Means on core). *The clustering accuracy of K-Means on these points is 0.87, up from an initial 0.51.*

Non-linearity in the outer layers: While the cores are separable by K-Means, we observe that as we include the outer layers, the performance of K-Means degrades. This can be attributed to the fact that the shape of the data becomes more non-linear as we move away from the center. We provide a detailed account of these observations in the supplementary material. We observe that as we move away from the center, shortest-path-distance on a nearest-neighbor embedding becomes an increasingly better estimate of cluster membership compared to the Euclidean distance. However, shortest-path-based approaches can be computationally expensive even with approximations [LMM20, THL23].

Instead, we exploit the density structure and build a graph that allows us to *efficiently* cluster the rest of the points building on our third model assumption that cluster membership of points in outer layers are better captured by nearby points in inner layers.

2.1.3 Step 3: Creating the Core Directed Nearest Neighbor (CDNN) graph

Our model assumption dictates that for any point in $\hat{\mathcal{L}}_{i,j}$, it will be close to points of the neighboring inner layer of the same ground truth cluster, irrespective of other distances. This motivates the following graph embedding.

Definition 2 (Centrally directed nearest neighbor graph (CDNN) $G_{(t,S)}^+$). *For every datapoint in S_j (the layers obtained in the previous step), we connect it to some t nearest neighbors in $\cup_{j'=0}^{j-1} S_{j'}$.¹*

We observe that distance on the CDNN graph is also more reliable than Euclidean distances. However, due to the layer-wise structure of the CDNN graph, we are able to devise a very fast algorithm to cluster the rest of the points.

2.1.4 Step 4: Expanding the clustering in a layer-wise manner

We instead expand the clustering a layer at a time. That is, given a clustering of the points in S_0 , we label the points in S_1 using the edges going from S_1 to S_0 , continuing this process layer-wise.

For this, we need two ingredients. First, for each point in S_0 , we define a k -dimensional vector \mathcal{C} (each entry corresponding to a cluster) that gives us the membership value of the point to the cluster according to the clustering algorithm we apply to the core. For example, it can be the distance to the k centroids for K-Means.

Next, we define a weight function for each edge in $G_{t,S}^+$ that is inversely proportional to the distance. For this paper we use UMAP’s weight function [MHM18], and observe the behavior w.r.t. different choices in the supplementary material. We use these two vectors to cluster the subsequent layers one at a time, which we describe in algorithm 3. Finally, we record the computational efficiency of this step.

Theorem 2. *Given the CDNN graph $G_{t,S}^+$ and a clustering of S_0 , the rest of the points can be clustered in $\mathcal{O}(n \cdot k \cdot t)$ time, which is linear in the number of the edges and the number of clusters in $G_{t,S}^+$.*

¹Ideally, we want a graph that connects vertices in S_j to vertices in S_{j-1} , but we choose the aforementioned formulation to limit propagation of error in the FlowRank outcome.

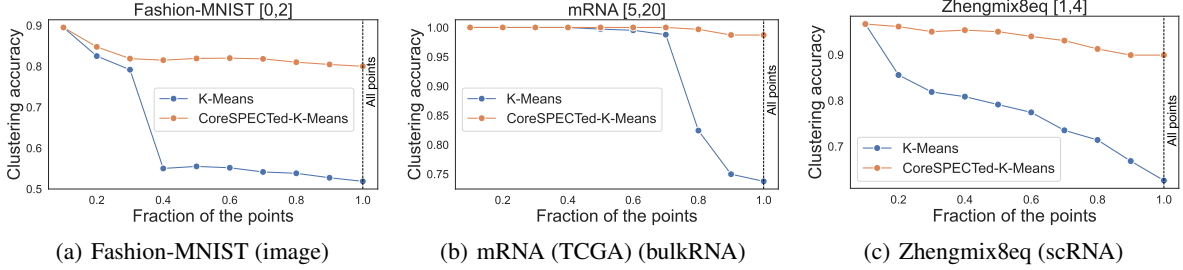


Figure 4: Comparing the accuracy of applying K-Means on the top x -fraction of the points (according to FlowRank) vs. applying K-Means to top 10% and then applying Layer-wise expansion (Algorithm 3) up to top x -fraction, for $x \in [0.1, 0.2, \dots, 1]$ for some pairs of clusters. For $x = 0.1$ (the cores), K-Means has very good performance, but as we apply K-Means on the outer layers, its performance deteriorates. In contrast, the layer-wise propagation gives significantly better response, further justifying our layer-wise model and utility of our framework.

Algorithm 3 Layer-wise-expansion of clustering: $\text{Expansion}(S, G^+, W, \mathcal{C})$

Inputs: The CDNN graph $G_{t,S}^+$ (with weight matrix W), layers S , cluster membership vector $\mathcal{C} : S_0 \rightarrow \mathbb{R}^k$.
 Initiate clustering: $V_1, \dots, V_k : \forall \mathbf{x} \in S_0, \mathbf{x} \in V_t : t := \arg \min_i \mathcal{C}[\mathbf{x}]_i$.
 Define data structure $\hat{\mathcal{C}} : \forall \mathbf{x} \in S_0, \hat{\mathcal{C}}(\mathbf{x}) \leftarrow \mathcal{C}(\mathbf{x})$
for $j \in 1 : \ell$ **do**
 for $\mathbf{u} \in S_j$ **do**
 $\hat{\mathcal{C}}(\mathbf{u}) \leftarrow \sum_{v \in N_{G^+}} W(\mathbf{u}, \mathbf{v}) \cdot \hat{\mathcal{C}}(\mathbf{v}); \quad k_u \leftarrow \arg \min \hat{\mathcal{C}}(\mathbf{u}); \quad V_{k_u} \leftarrow V_{k_u} \cup \mathbf{u}$
 end for
end for
return Clustering V_1, \dots, V_k

2.2 Combining the framework explicitly for K-Means

Here, we write down the different steps of our framework when applied to K-Means as Algorithm 4.

Algorithm 4 CoreSPECTed-K-means

Inputs: Dataset X and number of clusters k , hyperparameters: r, ℓ, t .

Step 1: Obtain $\Pi : X \rightarrow [0, 1]$ a random walk based estimate of the density of each point.
 $F \leftarrow \text{FlowRank}(X, \Pi, q, r)$ {Algorithm 2}
 $\forall j \in \{0, \dots, \ell - 1\}$, define S_j as the top $(j + 1)/\ell$ fraction of points as per F .

Step 2: Cluster S_0 with K-Means, obtaining centroids \mathbf{c}_i .
 Define cluster membership vector $\mathcal{C} : S_0 \rightarrow \mathbb{R}^k : \mathcal{C}(\mathbf{u}) = [\|\mathbf{u} - \mathbf{c}_i\|]_{1 \leq i \leq k}$

Step 3: Generate the CDNN graph $G_{t,S,X}^+$ and normalized weight matrix W {As per Definition 2}

Step 4: $V \leftarrow \text{Expansion}(S, G^+, W, \mathcal{C})$ {Algorithm 3}

return Clustering V_1, \dots, V_k

Theoretical guarantee of CoreSPECTed-K-Means. Finally, we note that as long as each of our steps is approximately correct, CoreSPECTed-K-Means almost correctly recovers the underlying clusters in data that follows our model, irrespective of the proximity of points in the outer layers.

Theorem 3 (Clustering in the LCPDM model). *Let X be n datapoints generated from the LCPDM(2, ℓ) model. Let us have an estimate of the density layers, given as $S_0, \dots, S_{\ell-1}$ such that $|S_j \cap \hat{\mathcal{L}}_j| = (1 - f)|\hat{\mathcal{L}}_j|, j > 0$. for a sufficiently small function $f = o(1)$ that is layer preserving. Then, applying a variant of K-Means to S_0 and expanding*

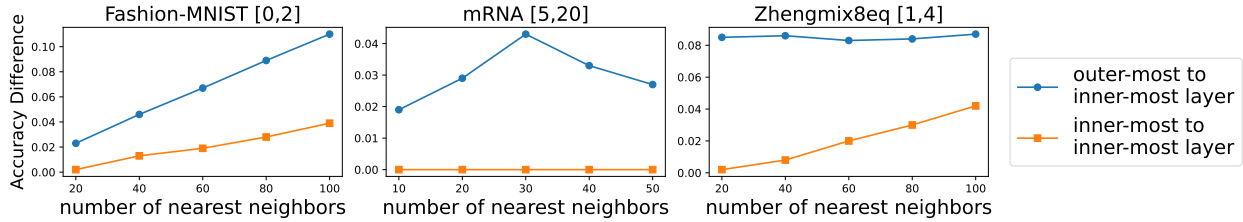


Figure 5: We first sort the nodes by the FlowRank values and select the nodes that are in the top and bottom 20% which we call the nodes from the inner-most and outer-most layers. Then we find the nearest neighbors using Euclidean distance and the shortest path distance in the CDNN graph generated. We show an empirical evidence that the periphery nodes exhibit more non-linear and the core nodes exhibit more euclidean structure by showing the differences of the nearest neighbor label accuracies.

the clustering using a CDNN graph (with correctly chosen parameters) results in clustering with $o(1)$ misclassification error rate on expectation.

While we obtain theoretical justification for our framework, obtaining these results under more generic conditions is an important next step. Additionally, studying the behavior of our framework in settings like Gaussian distribution supported on special kinds of manifolds is an interesting problem.

Computational efficiency We note that our framework is efficient. The main computation involves generating nearest neighbor graphs (both for initial density estimation as well as the CDNN graph generation), for which we used the ultra-fast HNSW [MY18] library for approximating the nearest neighbors. Our framework is also linearly dependent on k , the target number of clusters. For example, for CoreSPECTed-K-Means, our framework terminates in a few seconds for most of the datasets, taking around a minute for the TM dataset, which is a ≈ 50 -dimensional dataset consisting of $\approx 50,000$ points and 54 underlying clusters. We provide a detailed study of the run time (along with asymptotic runtime) of individual steps and scope for improvement in the supplementary material.

3 Statistical Evidence of the LCPDM model in real-world datasets

So far, we have provided initial theoretical support as well as various ablation study to better demonstrate the structural backgrounds and performance of our framework. Here, we provide some more statistical evidence that supports our model formulation and algorithm design. First we describe the datasets we use for evaluation.

Datasets We use a total of 15 datasets. We select the 11 single-cell datasets used by [MZ25] (obtained from [DRS18, AMC⁺19, SSG⁺19]), two popular bulk-RNA dataset from the The Cancer Genome Atlas Program (TCGA) [TCW15], and the popular image datasets MNIST [Den12] and Fashion-MNIST [XRV17]. The details of the datasets are provided in the supplementary material.

First, we show that the inner-most layers are indeed more Euclidean than the outer-most layer in terms of cluster-membership identities.

3.1 Nonlinearity of outer layers captured with relative accuracy of cluster-membership based on different distance measures

In figure 5, We first show the statistical evidence that further strengthens our claim that "the dense regions that are well-separated, while the surrounding outer layers exhibit more non-linear structure".

Specifically, we look at the cluster membership of some q nearest neighbors of points in the inner and outer layers via different notions of distances. To get a high resolution understanding, we focus on the same pairs of clusters that we used to observe the decaying performance of K-Means as points from outer layers were considered.

First, we look at the q nearest neighbors of core points among other core points. We consider the Euclidean distance and the shortest path on the K-NN graph distance. We record the difference in the fraction of intra-cluster points among nearest points according to different metrics. We observe that the accuracy for these two metrics remain relatively unchanged.

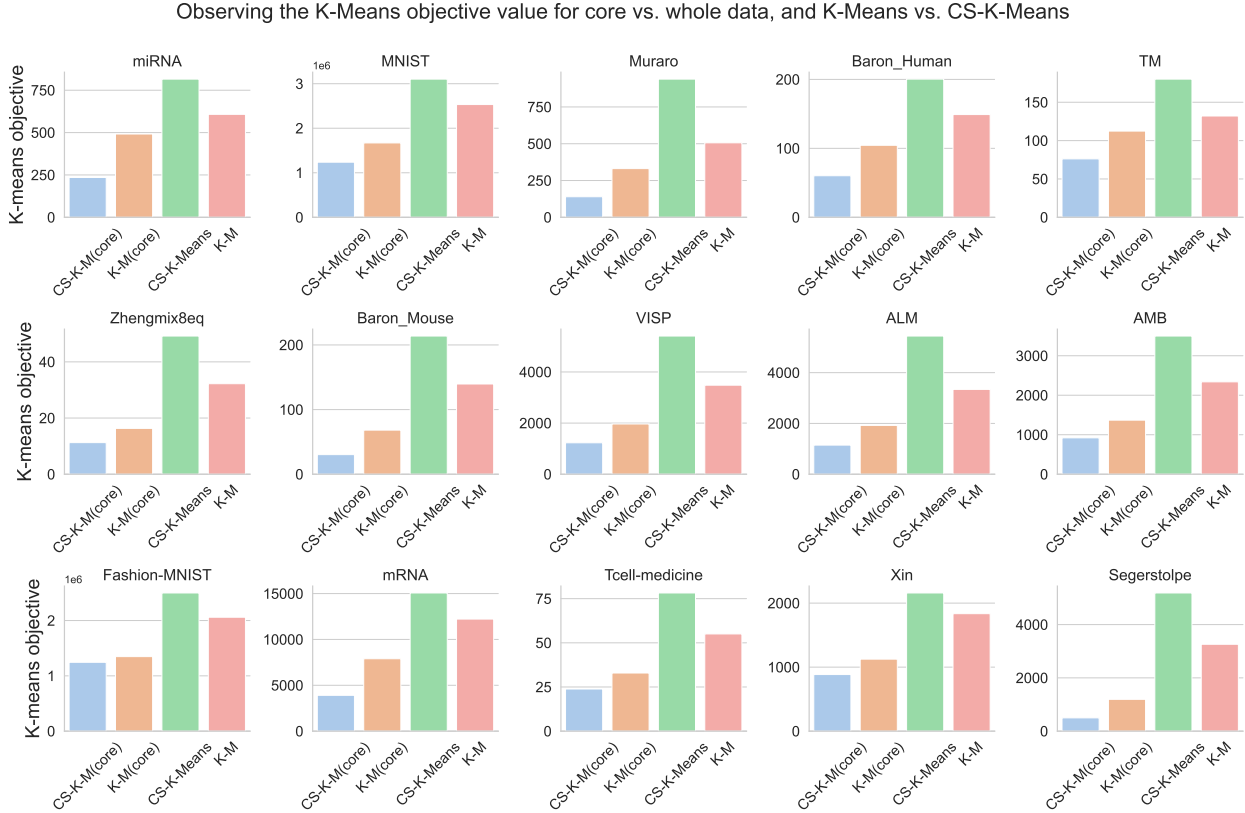


Figure 6: We observe that the K-Means objective of the clustering due to CS-K-Means is higher than that of K-Means when looking at the whole data. This contrasts with CS-K-Means having significantly better accuracy. This implies, for the whole dataset, linearly geometric objectives like that of K-Means is not suitable. However, if we focus only on the cores, a different picture emerges. The K-Means objective of the clusters among the core obtained by directly applying K-Means on core is smaller than that of the core-points when K-Means is applied on the whole dataset. This further strengthens the assumptions that the cores obtained by FlowRank are geometrically well-separated, contrasting the more complex geometry of the outer layers.

In comparison, we observe that if we look at the nearest neighbors of the outer-most layer among the cores, the intra-cluster accuracy according to Euclidean distance is relatively lower compared to shortest path on the CDNN graph that we generate. This implies, that the cluster-membership of the core-core points are well captured by Euclidean distance. In contrast, we need a more local-definition of distance (via shortest path on the CDNN graph) to get cluster-membership-preserving notions of distance.

3.2 Inversion in the behavior of K-Means objective value

We conclude this part with an interesting Phenomena on the K-Means objective value of the clustering obtained by K-Means and CoreSPECTed-K-Means. Essentially, we have the following observation.

1. **On the cores:** The K-Means objective value of the clustering obtained by K-Means on the core is lower than the K-Means objective value of the core points when K-Means was applied to the whole dataset.
2. **On the entire dataset:** Here, the K-Means objective value of CoreSPECTed-K-Means is higher than that of K-Means, even though the final clustering by CoreSPECTed-K-Means is of much higher quality, as we have observed.

We capture this in Figure 6. This further strengthens the assumptions that the cores obtained by FlowRank are geometrically well-separated, contrasting the more complex geometry of the outer layers.

4 Large scale experiments

So far, we have described our CoreSPECT framework, and showed the utility of the individual components via K-Means on two clusters of the Fashion MNIST dataset, along with some statistical phenomenon in comparison to K-means.

In this section, we extensively evaluate the performance of this framework on the aforementioned 15 datasets in comparison to well-known clustering algorithms. Furthermore, to demonstrate the generalization of its application, we also apply it to EM based fit of GMM [DLR77].

4.1 Improvement in K-Means and GMM due to CoreSPECT

Our framework only uses the clustering membership vector defined by any clustering algorithm of choice. For K-Means, we used the distance to the centers for each core point as entries of the vector. For GMM, when we it is applied to the core point, every point gets a k -long probability vector that determines the probability of the point being in one of the k clusters. We use the negative of that vector as the cluster membership vector. We first present some summary statistics on the improvement for K-Means and GMM due to the CoreSPECT framework.

Observation (Improvement due to CoreSPECT). *Over the 15 datasets, CoreSPECT improves the ARI of K-Means on 14/15 datasets, and NMI for 15/15 datasets with all parameters fixed to default. On average, ARI improves by 40.82% and NMI improves by 16.49%. Similarly, it improves the ARI and NMI of GMM by 13.75% and 4.24%, respectively.*

Here, we note that the improvement due to CoreSPECT is lower for the 4 smallest datasets (with less than 2500 points). In the supplementary material, we show that the performance of our framework can be further boosted with principled parameter selection methods including these small datasets.

4.2 Comparison with other algorithms

We have observed that our framework consistently improves the performance of K-Means and GMM. Next, we want to compare the relevance of the improved performance w.r.t. more complex density-based and geometry-based clustering algorithms.

We select three recent or/and popular Density Peak Clustering algorithms the original DPC [RL14], ADPclust [WX17], and a fast implementation of another popular DPC algorithm through a fast framework named PECANN [YEHS23]. Additionally we also use HDBSCAN [CMS13]. We also attempted to use DBSCAN [EKS⁺96] and OPTICS [ABKS99], but they categorized most points as outliers for most datasets so we omit them.

For Manifold clustering algorithms, we attempted to run the recent algorithms with theoretical guarantees by [LMM20] and [THL23]. However, we could not get a parameter initialization (after trying default and other suggested parameters) that gave better ARI or NMI than the vanilla Spectral Clustering (SC) on any of the datasets. Note that SC applies K-Means to the normalized spectral embedding of the nearest neighbor graph [VL07]. We also use bisecting K-Means [KKS00] as a hierarchical clustering algorithm.

	K-Means	CS-K-Means	GMM	PECANN	SC	HDBSCAN	Bi-K-Means	DP	ADPclust
ARI	4.93	2.27	3.27	<u>3.00</u>	3.40	6.00	6.20	7.67	8.00
NMI	5.13	<u>2.27</u>	3.60	3.07	2.07	6.33	6.73	7.60	7.93

Table 1: NMI and ARI rank of CoreSPECTed-K-Means on 15 datasets. The best value is in bold, and the second best is underlined

In Figure 1, we have shown the exact improvements in ARI due to CoreSPECTed-K-Means and CoreSPECT-GMM for 10 datasets. Here, we compare the performance over 15 datasets by demonstrating the average ranks for ARI (and NMI). As before, if we slightly tune the parameters for the small datasets, our performance further improves but in the interest of exhibiting robustness we use the same parameters for all datasets. We observe the rank of CoreSPECTed-K-Means compared to the other algorithms in Table 1. Similarly, we note the rank the CoreSPECTed-GMM also achieves the best ARI rank, and the second best NMI rank over all of the datasets. Furthermore, with slight parameter tuning, CoreSPECTed-K-Means is able to achieve also the best rank in NMI. We describe all of these results in the supplementary material.

4.3 Observing the power of CoreSPECT through noisy datasets

We have argued that the CoreSPECT works well for datasets where the data contains density layers as proposed in our model and the outer layers are not well separated in a Euclidean sense. To test this hypothesis further, we first

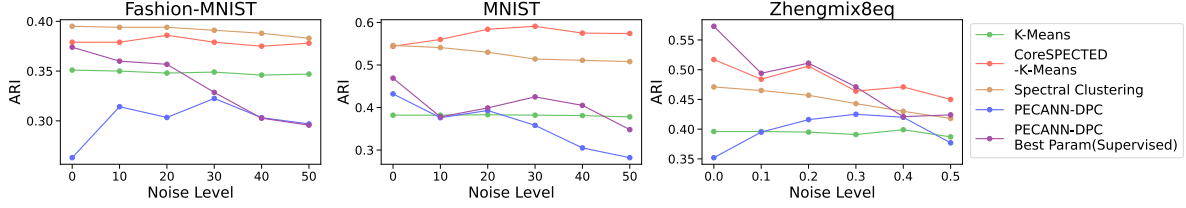


Figure 7: Comparative robustness of CoreSPECT enhanced K-Means on datasets with Gaussian perturbation. As the noise level increases, the performance of DPC deteriorates, with CoreSPECTed-K-Means demonstrating significantly higher resistance.

devise a controlled experiment by adding noise to a dataset. We use the image datasets MNIST, Fashion-MNIST and the popular single-cell dataset Zhengmix8eq. We use them as these are three datasets where all clusters are large. We add zero-mean isotropic Gaussian noise in a range that deteriorates the performance of all algorithms. For the image datasets, we choose variance in $\{10, 20, 30, 40, 50\}$, and for Zhengmix, in $\{0.1, \dots, 0.5\}$.

We compare the performance of K-Means, CoreSPECTed-K-Means (CS-K-Means), Spectral Clustering, PECANN-DPC with default parameters, and also, for a more adversarial comparison, we choose the parameters of PECANN-DPC that results in the best clustering. Note that this is a supervised choice. We call this PECANN-DPC (best param). We use this as for more adversarial comparison. The outcomes (in ARI) are shown in Figure 7.

We observe that DPC is the most affected by noise. For example, in the Zhengmix8eq dataset, PECANN-DPC with best parameters has higher ARI than our method in the noise-less case. However, as more noise is added, the performance deteriorates at a rate higher than CS-K-Means, eventually resulting in lower ARI. In comparison, both CS-K-Means and Spectral Clustering are more robust to noise, however, for both MNIST and Fashion-MNIST we appear to be more robust on average. This further highlights the strengths of our framework.

5 Ablation Studies

In the previous section we have demonstrated that our framework elevates the performance of both K-Means and GMM across 15 datasets, often outperforming recent density-peak-based and manifold-based clustering algorithms. In this section we provide several ablation studies, directed at understanding the importance of each of the steps in our framework. We start by recollecting the different steps in our framework on a high level in Figure 8

1. Step 1: Core (and subsequent density layers) extraction.

In this step we want to obtain the density layers in the data, such that the top-most layer contains the most separable cores and the subsequent layers contain more complex and less separable peripheral points.

As we have described in the main paper, we design an algorithm that we call FlowRank and then define the deciles as the layers. We aim to find the relatively dense regions of the data to obtain the cores of each cluster. Our method is inspired by the concept of relative centrality in [MZ25].

2. Step 2: Clustering the core.

In this step, the cores (S_0) are clustered with a simple algorithm of user's choice. We use K-Means for this part.

3. Step 3 and 4: Expanding the clustering to the rest of the points

We do this in two steps.

Step 3: Core directed nearest neighbor (CDNN) graph construction. Here, we design a layer-by-layer nearest neighbor graph structure using the estimated density layers.

Step 4: Layer-wise expansion of clustering. Finally, we use the clustering of the cores and the CDNN graph to cluster the rest of the points.

The key idea here is that our model dictates that the cluster membership of a point in a density layer is best determined to its proximity to points in an inner layer (as opposed to overall proximity to points).

Figure 8: The CoreSPECT Framework (on a high level)

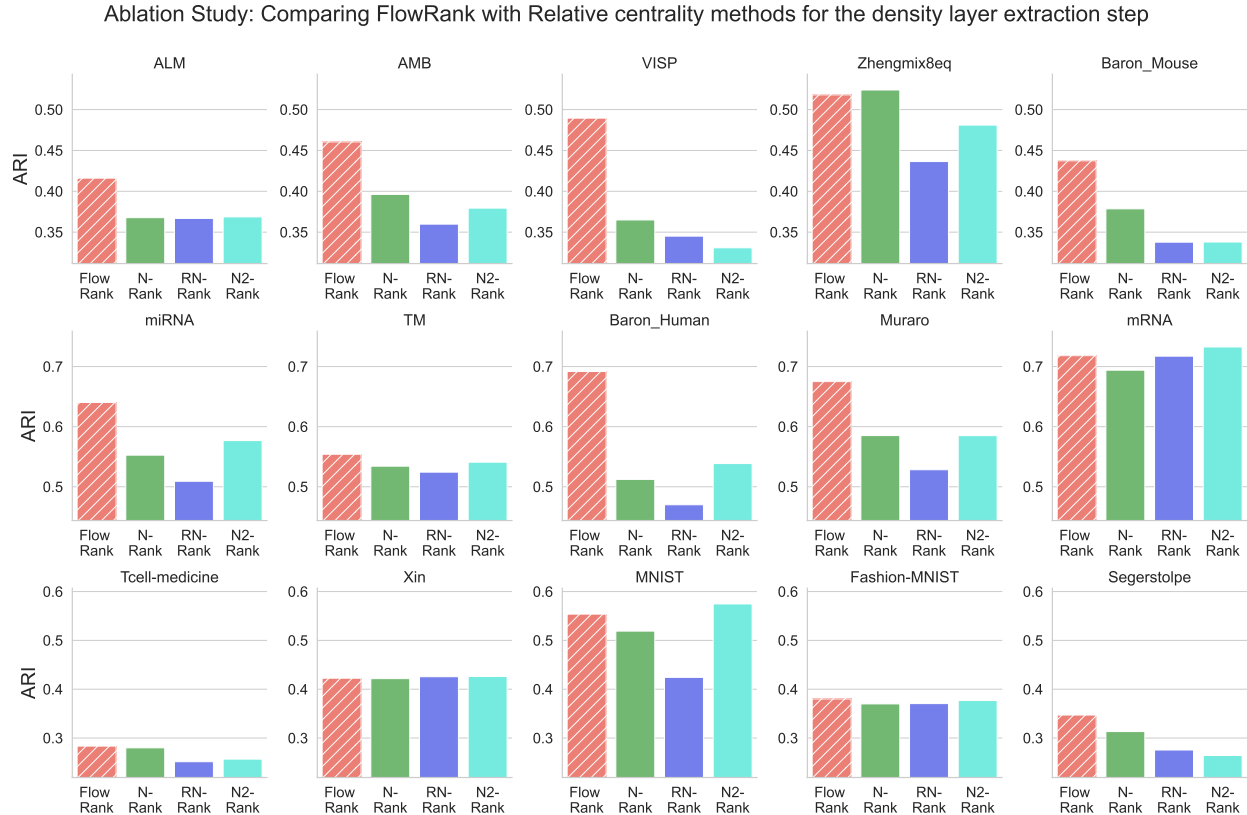


Figure 9: Contrasting the performance (ARI) of FlowRank with that of Relative centrality methods in the density-layer-extraction step of CoreSPECT. In 11 out of 15 datasets, FlowRank produces the best result, and is within 2% of the best in the other four datasets.

5.1 Approximating the density layers: Comparing FlowRank with relative-centrality methods.

We have discussed in Section B.3 that for some the small datasets, FlowRank fails to add points from the smallest clusters to the cores even when they are well-separated, and identified it as avenue for improvement. In this direction, we compare the merits of FlowRank w.r.t. the concept *relative-centrality* [MZ25] from where we drew inspiration. In [MZ25], the authors focus on K-NN graph embeddings of biological datasets, and then define ranking algorithms such that

- i) Top ranked points are better separable into their ground truth clusters compared to the whole data. They verify separability based on what fraction of edges in the induced subgraph of the top-ranked points are *intra-community*.
- ii) The top ranked points contain points from all clusters

They verify this property for 11 single-cell datasets (that we also use in our paper). The two properties sought by [MZ25] seems to fit our needs exactly. That is, if the top-ranked points are more separable and we have points from all underlying ground truth clusters, we will be able to obtain a high quality clustering of these points. However, crucially, we have a more specific requirement, which is **the core points should be geometrically well separated**. Note that this is not automatically ensured by the relative centrality methods. Indeed, a look at the algorithms in [MZ25] suggests that they aim to obtain locally-high-centrality points. While these points themselves may be better separable, they may be from very different parts of the space, and therefore, the performance of simple Geometric clustering algorithms like K-Means may not be good. To further investigate this hypothesis, we run our experiments by replacing FlowRank with algorithms of [MZ25]. We capture the results in Figure 9.

We observe that FlowRank usually leads to the best result, with significant advantage over the relative centrality methods in 10 out of 15 datasets, while being very similar to the best relative centrality method per-dataset for each of the other 5 datasets.

Ablation Study: Comparing our layer-expansion method with that of label propagation methods from semi-supervised-learning

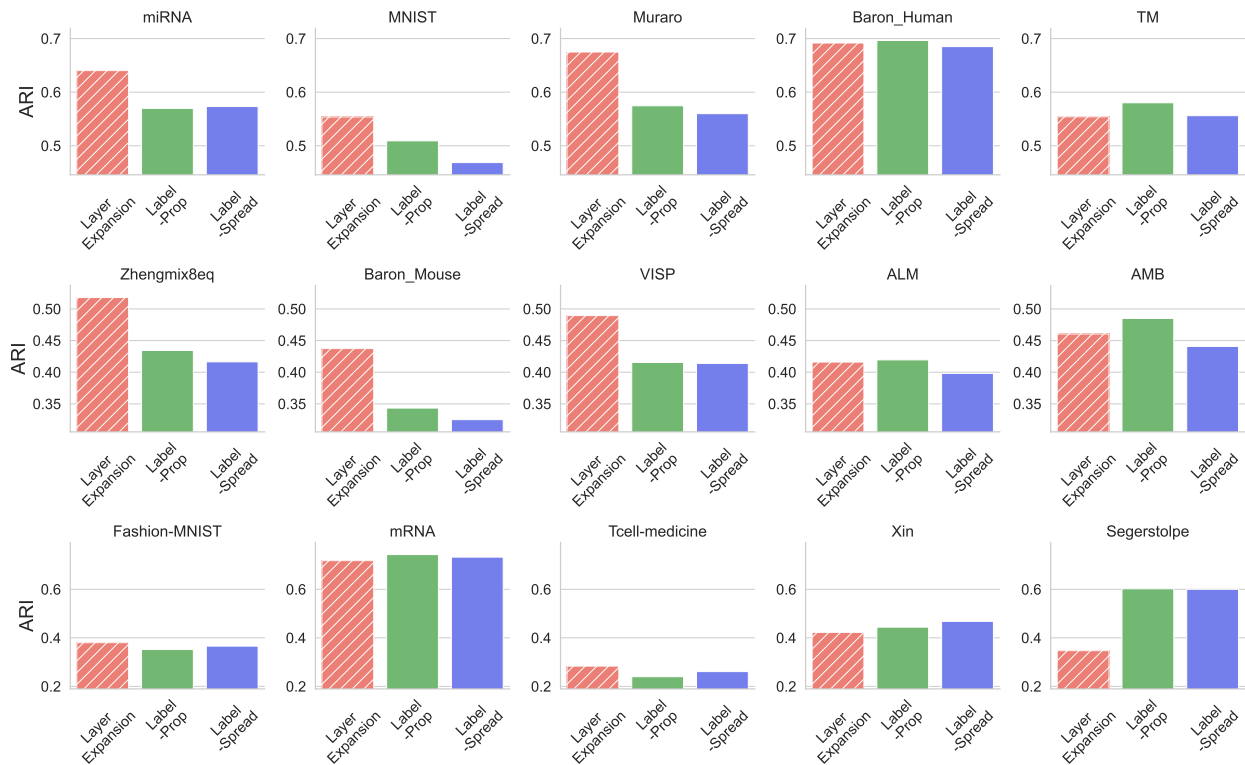


Figure 10: Contrasting the performance of CDNN graph generation+layer expansion with that of popular label propagation algorithms used in Semi supervised learning. Overall, our CDNN-graph based approach has the best rank, with noticeably better performance in 6 out of 15 datasets. We have almost identical performance in 7 more datasets, with doing noticeably worse in only one dataset (Segerstolpe).

Essentially, the reason behind this is that the relative centrality methods treat the K-NN graphs to have a single-layer core-periphery structure. However, we find that there are multiple density layers in the real world data, which necessitates our algorithm. However, we believe it is possible further improve our ranking and overall density-layer estimation algorithm, which we consider it as an important future direction.

5.2 Layer-wise propagation: A connection (and comparisons) of layer-wise-expansion to semi-supervised learning.

Next, we discuss a very obvious yet interesting connection between our framework and *semi supervised learning*.

In our framework, after we extract the cores and cluster them (which we expect and observe to have high correctness), we use this clustering to extend this to the rest of the data. This is very similar to the concept of *label propagation* [XZ02, ZBL⁺03], which is one of the fundamental approaches to semi-supervised learning (SSL). In SSL, given the true labels of some of the points, one wants to label the rest of the points. Therefore, our algorithm can be considered as some sort of a pseudo-semi-supervised-learning framework. This raises the following question.

Question 1. *Can SSL based label-propagation methods extend the clustering of the core as well as our CDNN graph based approach?*

In this direction, we look at popular two scikit-learn method, called Label-propagation [XZ02] and Label-spreading [ZBL⁺03]. The first is a “hard-clamping” method. That is, the initial labels provided by to the algorithm are never altered. In contrast, Label-spreading is a “soft-clamping” method, where it may readjust some of the initial labels. In short, both the methods aim to create some affinity matrix from the labeled points to the rest of the data. In this direction, the original papers defined an rbf-based kernel for this purpose, which is also the default setting in the scikit-learn implementation. We first tried these two methods to enhance the clustering of the cores by K-Means. Here,

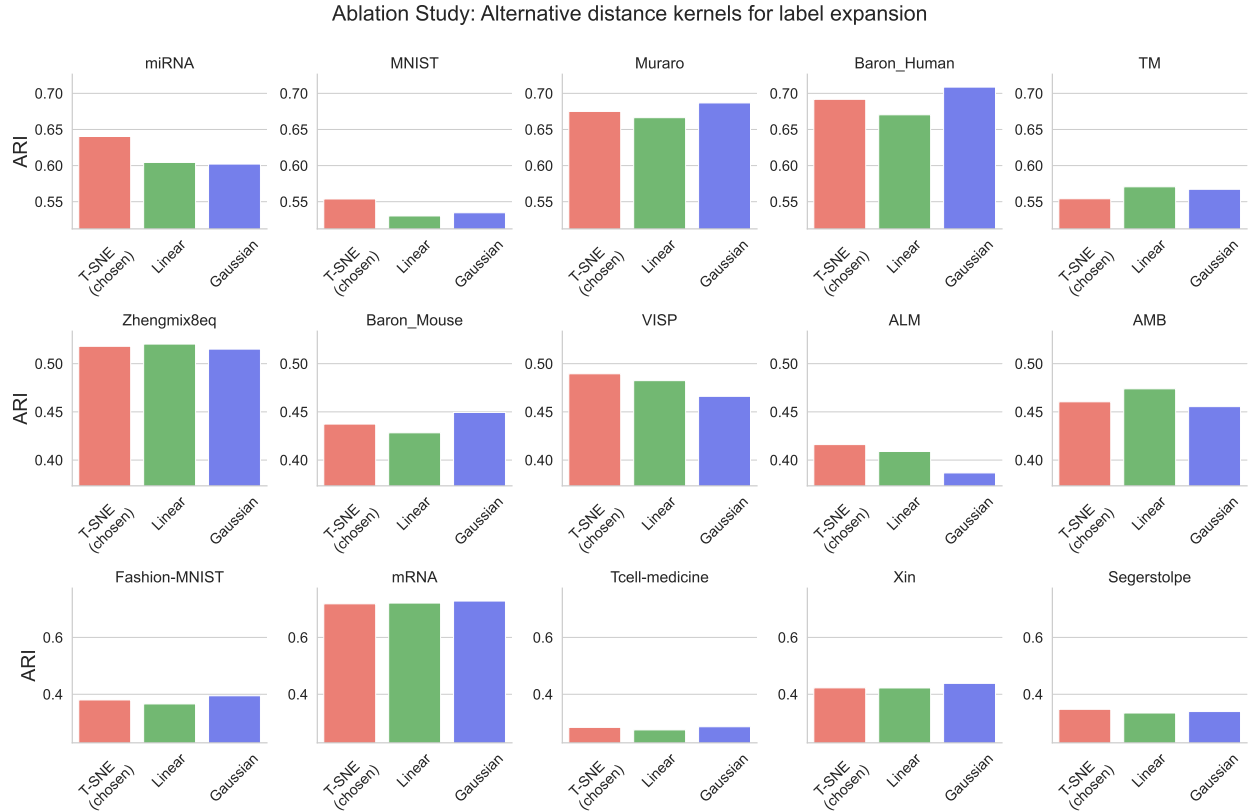


Figure 11: Performance of CoreSPECTed-K-Means for different choice of weight matrix for the layer-expansion

we observe that both for label-propagation and label-spreading methods fail, resulting in significantly NMI and ARI compared to K-Means on the whole dataset.

K-NN-based SSL label-propagation algorithms To further investigate the possibility of using SSL based propagation, we use the alternative kernel that uses only nearest neighbors to propagate the initial labels, performing this recursively until all the points are labeled. We place the ARI values of using Label-propagation and label-spread instead of our layer-expansion idea in Figure 10.

We observe that for this setting, both SSL methods perform well, resulting in ARI that is higher than K-Means on the whole dataset in most cases. Overall, our CDNN-based approach still performs the best (except in the Segerstolpe dataset, where both the SSL methods have much better performance). This is a reasonable outcome, as for datasets that are good fit for our density-layer-structure, the cores obtained by FlowRank are the points in the inner-most layers. In contrast, in SSL one often wants to labels from *all regions* of the data, which SSL based labale propagation ideas aim to implicitly exploit.

Ignoring the Segerstolpe dataset (which as we have discussed, does not contain a strong density-layer structure), our approach leads to roughly 7% higher ARI than label-prop and 8% higher than label-spread. On one hand, this further justifies our model formulation and algorithmic framework. On the other hand, this opens up the possibility of further improving our framework by incorporating ideas from more advanced SSL ideas.

We believe better understanding the applicability of such label propagation ideas and appropriating for our framework may lead to even better performance, which is an exciting future direction.

5.3 Choice of weight matrix in the layer-expansion approach.

Next, we briefly recall the structure of our layer-expansion procedure. After we have partitioned the points into deciles (using the FlowRank ranking), for any point in the j -th layer, we find nearest neighbors among the points upto $j - 1$ -th layer (which have been already labeled) and then decide a (normalized) weight function on these edges such that the cluster membership vector of the new point is a weighted sum of the cluster membership vectors of its neighbors. In

the results in our main paper, we have used the weight function of UMAP [MHM18] (which itself is inspired from t-SNE [VdMH08]) to decide these weights.

Here we perform an ablation study to understand the variability in the performance of CoreSPECT based on the weight function itself (using K-Means as the core-clustering algorithm). We describe the methods we use below.

1. **Chosen setting:** Given a points \mathbf{x} and some t neighbors Z_t , the weight of an edge $\mathbf{x} \rightarrow \mathbf{x}'$ is decided as $W(\mathbf{x}, \mathbf{x}') = \exp\left(\frac{\|\mathbf{x} - \mathbf{x}'\| - \min_{\mathbf{u} \in Z_t} \|\mathbf{x} - \mathbf{u}\|}{\sigma_x}\right)$ such as the sum of all weights is a fixed constant (this is achieved by choosing a different σ_x for each \mathbf{x}).
2. **Linear kernel:** In this setting, we simply choose $W(\mathbf{x}, \mathbf{x}') = \frac{1}{1 + \|\mathbf{x} - \mathbf{x}'\|}$
3. **Global Gaussian kernel:** This is similar to our chosen setting, without choosing a different σ_x for each point. $W(\mathbf{x}, \mathbf{x}') = \exp\left(\frac{\|\mathbf{x} - \mathbf{x}'\| - \min_{\mathbf{u} \in Z_t} \|\mathbf{x} - \mathbf{u}\|}{\sigma_x}\right)^2$

In Figure 11, we present the performance of the different distance kernels. We observe that overall, the t-SNE kernel has very slight advantage over the two methods, being better than linear kernel in 10/15 datasets, and Gaussian kernel in 8/15 datasets. However, we note that the overall differences in the three methods are negligible for most datasets.

6 Limitations and Future Directions

We conclude with a discussion on our limitations.

1. The main strength of the paper is also its primary limitation. We exploit a correlation in the geometry-density structure of the data, but this implies our framework is only applicable to such datasets. While we observe our framework is consistently applicable on large and poorly separated datasets, a notion for estimating when data fits our model is crucial for real-world application.
2. A second limitation lies in the core-extraction step, as previously noted. We use the order provided by FlowRank and partition it into ten parts. Ideally, different data will have different numbers of layers for different clusters, and this phenomena needs to be explored further. We believe FlowRank is only a placeholder, and an improved algorithm can be achieved.
3. Next, we note that we have achieved the gains mentioned so far by fixing the other hyperparameters of our framework. However, we believe these hyperparameters can be more informatively selected that can further boost our performance.
4. We have applied our framework to two algorithms. Applying and understanding the effect of our framework on different algorithms and different kind of embeddings is necessary to better understand the scope of application.
5. Data-based selection of the optimal hyper-parameter is an important direction. As we have observed, some of the optimal parameters depend on the internal geometry of the data. For example, the correct radius for choosing neighbors for ascending random walk depends on the width of the layers. A better inference of this underlying geometry may further raise confidence in our framework.
6. In this paper, we have looked at four manifold clustering algorithm, but were able to only find one (the K-NN graph based spectral clustering) that provided competitive results. Comparing the performance of other manifold clustering algorithm is important to further understand the scope of the improvement our framework provides.

Our framework and algorithms also stand to benefit from further theoretical insight. For example, we believe it will be possible to prove that FlowRank provides a layer-preserving ranking under our current assumptions. Similarly, better understanding the scope and limitations of the assumptions we make in the paper is also important. Here we note that the primary focus of this paper is not theoretical completion. Rather, we use theoretical insights of our model to create a generic framework which we apply to many datasets, on multiple methods, which we also compare with many clustering algorithms as well as provide various ablation studies that signify the importance and influence of the individual component of our framework.

References

- [ABKS99] Mihael Ankerst, Markus M Breunig, Hans-Peter Kriegel, and Jörg Sander. Optics: Ordering points to identify the clustering structure. *ACM Sigmod record*, 28(2):49–60, 1999.
- [AMC⁺19] Tamim Abdelaal, Lieke Michielsen, Davy Cats, Dylan Hoogduin, Hailiang Mei, Marcel JT Reinders, and Ahmed Mahfouz. A comparison of automatic cell identification methods for single-cell rna sequencing data. *Genome biology*, 20:1–19, 2019.
- [AV06] David Arthur and Sergei Vassilvitskii. k-means++: The advantages of careful seeding. Technical report, Stanford, 2006.
- [BLW19] Jean-Daniel Boissonnat, André Lieutier, and Mathijs Wintraecken. The reach, metric distortion, geodesic convexity and the variation of tangent spaces. *Journal of applied and computational topology*, 3:29–58, 2019.
- [BTS⁺21] Serguei Barannikov, Ilya Trofimov, Grigorii Sotnikov, Ekaterina Trimbach, Alexander Korotin, Alexander Filippov, and Evgeny Burnaev. Manifold topology divergence: a framework for comparing data manifolds. *Advances in neural information processing systems*, 34:7294–7305, 2021.
- [CMS13] Ricardo JGB Campello, Davoud Moulavi, and Jörg Sander. Density-based clustering based on hierarchical density estimates. In *Pacific-Asia conference on knowledge discovery and data mining*, pages 160–172. Springer, 2013.
- [Den12] Li Deng. The mnist database of handwritten digit images for machine learning research [best of the web]. *IEEE signal processing magazine*, 29(6):141–142, 2012.
- [DLR77] Arthur P Dempster, Nan M Laird, and Donald B Rubin. Maximum likelihood from incomplete data via the em algorithm. *Journal of the royal statistical society: series B (methodological)*, 39(1):1–22, 1977.
- [DRS18] Angelo Duò, Mark D Robinson, and Charlotte Soneson. A systematic performance evaluation of clustering methods for single-cell rna-seq data. *F1000Research*, 7, 2018.
- [EKS⁺96] Martin Ester, Hans-Peter Kriegel, Jörg Sander, Xiaowei Xu, et al. A density-based algorithm for discovering clusters in large spatial databases with noise. In *kdd*, volume 96, pages 226–231, 1996.
- [Fed59] Herbert Federer. Curvature measures. *Transactions of the American Mathematical Society*, 93(3):418–491, 1959.
- [HSL⁺23] Lukas Heumos, Anna C Schaar, Christopher Lance, Anastasia Litinetskaya, Felix Drost, Luke Zappia, Malte D Lücken, Daniel C Strobl, Juan Henao, Fabiola Curion, et al. Best practices for single-cell analysis across modalities. *Nature Reviews Genetics*, 24(8):550–572, 2023.
- [KKS00] Michael Steinbach, George Karypis, Vipin Kumar, and Michael Steinbach. A comparison of document clustering techniques. In *TextMining Workshop at KDD2000 (May 2000)*, pages 428–439, 2000.
- [Llo82] Stuart Lloyd. Least squares quantization in pcm. *IEEE transactions on information theory*, 28(2):129–137, 1982.
- [LMM20] Anna Little, Mauro Maggioni, and James M Murphy. Path-based spectral clustering: Guarantees, robustness to outliers, and fast algorithms. *Journal of machine learning research*, 21(6):1–66, 2020.
- [LRSH⁺24] Yingcong Li, Ciro Ramírez-Suástegui, Richard Harris, Francisco Emmanuel Castañeda-Castro, Gabriel Ascui, Tamara Pérez-Jeldres, Alejandro Diaz, Carla Morong, Daniel A Giles, Jiani Chai, et al. Stem-like t cells are associated with the pathogenesis of ulcerative colitis in humans. *Nature Immunology*, pages 1–14, 2024.
- [MHA17] Leland McInnes, John Healy, and Steve Astels. hdbscan: Hierarchical density based clustering. *The Journal of Open Source Software*, 2(11):205, 2017.
- [MHM18] Leland McInnes, John Healy, and James Melville. Umap: Uniform manifold approximation and projection for dimension reduction. *arXiv preprint arXiv:1802.03426*, 2018.
- [MY18] Yu A Malkov and Dmitry A Yashunin. Efficient and robust approximate nearest neighbor search using hierarchical navigable small world graphs. *IEEE transactions on pattern analysis and machine intelligence*, 42(4):824–836, 2018.
- [MZ25] Chandra Sekhar Mukherjee and Jiapeng Zhang. Balanced ranking with relative centrality: A multi-core periphery perspective. In *ICLR*, 2025.
- [NSW08] Partha Niyogi, Stephen Smale, and Shmuel Weinberger. Finding the homology of submanifolds with high confidence from random samples. *Discrete & Computational Geometry*, 39:419–441, 2008.

- [RL14] Alex Rodriguez and Alessandro Laio. Clustering by fast search and find of density peaks. *science*, 344(6191):1492–1496, 2014.
- [SM00] Jianbo Shi and Jitendra Malik. Normalized cuts and image segmentation. *IEEE Transactions on pattern analysis and machine intelligence*, 22(8):888–905, 2000.
- [SSG⁺19] Stephen J Smith, Uygur Sümbül, Lucas T Graybuck, Forrest Collman, Sharmishta Seshamani, Rohan Gala, Olga Gliko, Leila Elabbady, Jeremy A Miller, Trygve E Bakken, et al. Single-cell transcriptomic evidence for dense intracortical neuropeptide networks. *elife*, 8:e47889, 2019.
- [SVY⁺18] Peter Savas, Balaji Virassamy, Chengzhong Ye, Agus Salim, Christopher P Mintoff, Franco Caramia, Roberto Salgado, David J Byrne, Zhi L Teo, Sathana Dushyanthen, et al. Single-cell profiling of breast cancer t cells reveals a tissue-resident memory subset associated with improved prognosis. *Nature medicine*, 24(7):986–993, 2018.
- [TCW15] Katarzyna Tomczak, Patrycja Czerwińska, and Maciej Wiznerowicz. Review the cancer genome atlas (tcga): an immeasurable source of knowledge. *Contemporary Oncology/Współczesna Onkologia*, 2015(1):68–77, 2015.
- [THL23] Nicolas Garcia Trillos, Pengfei He, and Chenghui Li. Large sample spectral analysis of graph-based multi-manifold clustering. *Journal of Machine Learning Research*, 24(143):1–71, 2023.
- [VdMH08] Laurens Van der Maaten and Geoffrey Hinton. Visualizing data using t-sne. *Journal of machine learning research*, 9(11), 2008.
- [VL07] Ulrike Von Luxburg. A tutorial on spectral clustering. *Statistics and computing*, 17:395–416, 2007.
- [WX17] Xiao-Feng Wang and Yifan Xu. Fast clustering using adaptive density peak detection. *Statistical methods in medical research*, 26(6):2800–2811, 2017.
- [XRV17] Han Xiao, Kashif Rasul, and Roland Vollgraf. Fashion-mnist: a novel image dataset for benchmarking machine learning algorithms. *arXiv preprint arXiv:1708.07747*, 2017.
- [XZ02] Zhu Xiaojin and Ghahramani Zoubin. Learning from labeled and unlabeled data with label propagation. In *Tech. Rep., Technical Report CMU-CALD-02-107*. Carnegie Mellon University, 2002.
- [YEHS23] Shangdi Yu, Joshua Engels, Yihao Huang, and Julian Shun. Pecann: Parallel efficient clustering with graph-based approximate nearest neighbor search. *arXiv preprint arXiv:2312.03940*, 2023.
- [YLL12] Miin-Shen Yang, Chien-Yo Lai, and Chih-Ying Lin. A robust em clustering algorithm for gaussian mixture models. *Pattern Recognition*, 45(11):3950–3961, 2012.
- [ZBL⁺03] Dengyong Zhou, Olivier Bousquet, Thomas Lal, Jason Weston, and Bernhard Schölkopf. Learning with local and global consistency. *Advances in neural information processing systems*, 16, 2003.

A Model and Proofs

In this Section, we will describe our Layered-core-periphery-density-model LCPDM(k, ℓ) model in further detail and provide initial theoretical support to some of the steps described in the main paper. In doing so, we will also obtain some insights into the different parameters of our algorithm. First we describe the configuration of our model in detail.

A.1 The LCPDM(k, ℓ) model

As we have described, we have some assumptions on the density and some on the geometry. Here, we describe them in greater detail. We assume points of each ground-truth cluster i is being generated from some $\mathcal{X}_i \in \mathbb{R}^d$. We make the following assumptions on the geometry-density interaction. For the rest of the discussion we focus on the case of $k = 2$. First, we formally define the reach of a manifold, which we use to derive different results.

Definition 3 ([Fed59]). *The reach of a set S is defined as the infimum of distances between points in S and points in its medial axis, the points in ambient space for which there does not exist a unique closest point in S .*

Detailed model formulation

1. *Globally flat manifold:* We assume the sets \mathcal{X}_0 and \mathcal{X}_1 lie on a flat m -dimensional smooth manifold \mathcal{M} , i.e., $\mathcal{X}_0 \cup \mathcal{X}_1 \subset \mathcal{M}$ with a reach of τ for a fixed m .

2. *Concentric sub-manifolds (with well-defined width):* The fundamental assumption we make is that \mathcal{X}_i can be expressed as a hierarchy of concentric sub-manifolds $\mathcal{X}_{i,0} \subset \mathcal{X}_{i,1} \subset \dots \subset \mathcal{X}_{i,\ell-2} \subset \mathcal{X}_{i,\ell-1} = \mathcal{X}_i$. Recall that we define $\mathcal{L}_{i,j} = \mathcal{X}_{i,j} \setminus \mathcal{X}_{i,j-1}$.

These concentric sub-manifolds are then defined in the following way. We start with a $\mathcal{X}_{i,0}$ with reach $\tau_{i,0}$. Then, the super-sets are defined as

$$\mathcal{X}_{i,j+1} = \{x : x \in \mathcal{M}, d_{\mathcal{M}}(x, \mathcal{X}_{i,j}) < f_{i,j}(x)\}$$

where $f_{i,j} : \mathcal{M} \rightarrow \mathbb{R}$ is a smooth function with $\Delta_{i,j}^{\min} \leq f_{i,j}() \leq \Delta_{i,j}^{\max}$, defining the minimum and maximum width of the layer $\mathcal{L}_{i,j}$. Furthermore, Each layer $\mathcal{L}_{i,j}$ has a reach of $\tau_{i,j}$.

Density assumptions: Each community has a density hierarchy, with the most densest layer being the central one, and the layers being progressively less dense. This is realized as follows. The data is generated by sampling $n_{i,j}$ points from each layer $\mathcal{L}_{i,j}$ uniformly at random, such that there exists a constant $1 < C < 2$ satisfying

$$\frac{n_{i,j}}{\text{Vol}(\mathcal{L}_{i,j})} = C \cdot \frac{n_{i,j+1}}{\text{Vol}(\mathcal{L}_{i,j+1})}$$

We denote the points generated from $\mathcal{L}_{i,j}$ as $\hat{\mathcal{L}}_{i,j}$ and together let the points be called \hat{X} .

Geometric assumptions w.r.t. ground truth cluster

Assumption 1. 1. *Cores are well-separated. The first assumption on the geometry dictates that the core-layers of the clusters are well separated in an Euclidean sense. For any clusters i, i'*

$$\exists \mu < 0.5 \quad \text{s.t.} \quad \max_{\mathbf{x} \in \mathcal{L}_{i,0}, \mathbf{x}' \in \mathcal{L}_{i',0}} \|\mathbf{x} - \mathbf{x}'\| \leq \mu \cdot \min_{\mathbf{x} \in \mathcal{L}_{i,0}, \mathbf{x}' \in \mathcal{L}_{i',0}} \|\mathbf{x} - \mathbf{x}'\|$$

Furthermore, we assume $\min_{\mathbf{x} \in \mathcal{L}_{i,0}, \mathbf{x}' \in \mathcal{L}_{i',0}} \|\mathbf{x} - \mathbf{x}'\| \leq 0.5\tau$. This is to enforce the flatness of the underlying manifold.

However, note that the individual layers themselves may have smaller reach, and thus be harder to cluster using simple algorithms like K-Means.

2. *Layer-wise clustering membership alignment. There exists $\delta < 1$ such that for any $\mathbf{x} \in \mathcal{L}_{i,j}$ and any $i' \neq i$, $\min_{\mathbf{x}' \in \mathcal{L}_{i',j-1}} \|\mathbf{x} - \mathbf{x}'\| \leq \delta \cdot \min_{\mathbf{x}'' \in \mathcal{L}_{i',j-1}} \|\mathbf{x} - \mathbf{x}''\|$.*

In this direction, we prove three results to provide initial theoretical support to our algorithm. The consistent performance of our framework warrants a more in-depth analysis and understanding and refinement of the model to further understand and exploit these underlying structures, and we end the Section with a discussion on several such directions.

Against this backdrop, we prove three results. First, we prove that the cores can be clustered easily.

A.2 Clustering the cores

Here we formally define and prove Proposition 1 of Main paper. In fact, we show that for our definition, we do not need a multi-step K-Means++. Rather, we run *one-step* K-Means++ $\Theta(\log n)$ times, and select the outcome with the least K-Means objective score.

First we define the K-Means++ method of [AV06] in brief. In the case of $k = 2$, the centers are chosen as follows. The initial centroid is chosen randomly. Then, the second center is chosen as follows. Any datapoint u is chosen to be the second center with probability $\frac{\|u - c_1\|^2}{\sum_{v \in Y} \|v - c_1\|^2}$. That is, points are chosen with probability proportional to the squared distance to the center. Once the centers are chosen, the usual iterative K-Means algorithm is applied up to some step (or convergence).

Proposition (Restated Proposition 1). *Let n_0 and n_1 points ($n_0 > n_1$ WLOG) be sampled from $\mathcal{X}_{0,0}$ and $\mathcal{X}_{1,0}$ respectively such that $\mu n_0 \leq n_1$. These points are denoted $\hat{\mathcal{L}}_{0,0}$ and $\hat{\mathcal{L}}_{1,0}$. Consider the slightly modified K-Means algorithm. Obtain two centers using the K-Means++ method and run one-step K-Means. Repeat this process some $2 \log n$ times and accept the result with minimum K-Means objective value. This algorithm separates the two cores correctly with probability $1 - o(1)$.*

Proof. We condition on the event that the first center selected is from $\hat{\mathcal{L}}_{0,0}$. This happens with probability ≥ 0.5 (as it is the larger set).

Let, the minimum inter-community distance be α . Then, the maximum intra-community distance is $\mu \cdot \alpha$.

Then, the probability that the second center is a point from $\mathcal{X}_{1,0}$ is

$$\begin{aligned} \Pr(c_2 \in \mathcal{X}_{1,0}) &= \frac{\sum_{\mathbf{x} \in \hat{\mathcal{L}}_{1,0}} \|c_1 - \mathbf{x}\|^2}{\sum_{\mathbf{x} \in \hat{X}} \|c_1 - \mathbf{x}\|^2} \\ &= \frac{\sum_{\mathbf{x} \in \hat{\mathcal{L}}_{1,0}} \|c_1 - \mathbf{x}\|^2}{\sum_{\mathbf{x} \in \hat{\mathcal{L}}_{0,0}} \|c_1 - \mathbf{x}\|^2 + \sum_{\mathbf{x} \in \hat{\mathcal{L}}_{1,0}} \|c_1 - \mathbf{x}\|^2} \\ &\geq \frac{\alpha^2 \cdot n_1}{\mu^2 \alpha^2 n_0 + \alpha^2 n_1} \\ &\geq \frac{\alpha^2 n_1}{\mu \alpha^2 (\mu n_0) + \alpha^2 n_1} \\ &\geq \frac{\alpha^2 n_1}{\mu \alpha^2 n_1 + \alpha^2 n_1} \geq \frac{1}{\mu + 1} \end{aligned}$$

That is, with probability $\frac{1}{\mu+1}$, the two centers chosen belong to the different ground truth clusters. Let 1_i be the indicator variable for the i -th initialization that is 1 if the two centers are from two clusters. Then, we have

$$\Pr\left(\sum_{i=1}^{2 \log n} 1_i > 0\right) = 1 - (\Pr(1_i = 0))^{2 \log n} \geq 1 - \left(\frac{2\mu + 1}{2\mu + 2}\right)^{2 \log n} = 1 - o(1)$$

This shows that with high probability, one of the initialization will lead to two centers being chosen from two different ground truth clusters. Then, based on the distance definition, clustering the points by assigning each point to its closest center will lead to a solution with zero misclassification error.

Next, note that the K-Means objective of any solution with two centers being selected from the different ground truth cluster is smaller than the K-Means objective of any solution where both centers are selected from the same cluster. This is because of the following.

Case 1: The K-Means objective value if the two centers are selected from different clusters is upper bounded by $(\mu\alpha)^2(n_0 + n_1)$. This is assuming each point is farthest possible away from the centers.

Case 2: The K-Means objective value if both centers are selected from the same cluster is lower bounded by $\alpha^2 n_1$. This is assuming both centers are in the larger cluster $\mathcal{X}_{0,0}$ and the K-Means objective value w.r.t. the points in $\mathcal{X}_{0,0}$ is zero.

Then, we have

$$(\mu\alpha)^2(n_0 + n_1) \leq \mu\alpha^2 \cdot \mu n_0 + \mu^2 \alpha^2 n_1 \leq \mu\alpha^2 n_1 + \mu^2 \alpha^2 n_1 \leq (\mu + \mu^2)\alpha^2 n_1 \leq 0.75\alpha^2 n_1$$

This implies that the maximum K-Means objective value when the centers are chosen from different ground truth clusters is smaller than the minimum K-Means objective when the two centers are chosen from the same ground truth cluster. This, combined with the fact that with probability $1-o(1)$ one of the initializations selects centers from different ground truth clusters completes the proof. \square

A.3 Extracting the cores with FlowRank

Next, we prove that if the FlowRank algorithm were given the exact density value for each point (which we have assumed to be same for any Layer $\mathcal{L}_{i,j}$), FlowRank gives a score of 1 to all core points (points sampled from $\mathcal{L}_{i,0}$) and a score of < 1 to all non-core points. This gives us an initial insight into FlowRank’s functionality. If all the core points are valued 1 and all non-core points are valued at less than 1, then selecting all the 1-valued points will give us the cores, which can then be clustered as shown in Section A.2.

A.3.1 Conditions for core-score being 1

Recall that in FlowRank, after we have a density estimation of the points, we have an ascending random-walk step such that for each point u , we look at its some $r = \mathcal{O}(1)$ neighbors, and move to a neighbor with higher density value at random. We continue this process until we reach a maxima, and the FlowRank value of u is the ratio of the density of u and the average densities of the reachable density peaks. Then, we have the following argument.

Lemma 1. *If for any core point $\mathbf{x} \in \mathcal{L}_{0,0}$, all of its r neighbors are in \mathcal{X}_0 , the FlowRank score of \mathbf{x} is 1. Furthermore, in the general case, this is a necessary condition.*

Proof. This is because, as long as all the neighbors of \mathbf{x} are in $\mathcal{L}_{0,0}$, they are either another point in $\mathcal{L}_{0,0}$ with same density as \mathbf{x} or a point in $\mathcal{X}_{0,j}, j > 0$ with lower density. following the formulation of the model. This makes \mathbf{x} a local maxima of the walk itself. That is, any density-ascending random walk cannot take any step starting from \mathbf{x} , resulting in FlowRank score of \mathbf{x} being 1.

The necessity of this condition follows from the fact that we do not make any assumptions on the relation of densities of the layers from different clusters. Even if $\mathcal{L}_{0,0}$ is the highest density region in \mathcal{X}_0 , its density may be lower than the lowest density region in \mathcal{X}_1 . In such a case, if there is any of the r neighbors of a point in $\mathcal{L}_{0,0}$ is from \mathcal{X}_1 , that point will get a FlowRank score of less than 1. \square

Then, we want to prove that this condition indeed holds in our model. We first define some notations.

Definition 4. *We define $\sup d(S)$ as the maximum Euclidean distance between two points in a set S . Similarly, we define $\sup d(S, X, r)$ as the maximum distance to the r -th nearest neighbor of points in S in the Set X .*

In this direction, we first show that inter-core edges are impossible.

Proposition 2 (Inter-core edges are impossible). *Let \mathbf{x} be a point in $\mathcal{L}_{0,0}$. Then for any $r = \mathcal{O}(1)$, none of \mathbf{x} ’s r -closest neighbors are from $\mathcal{L}_{1,0}$.*

Proof. From the first condition in Assumption 1, we know that the maximum intra-core distance is μ times smaller than the minimum inter-core distance. As there are $\omega(r)$ many points in $\mathcal{L}_{0,0}$, none of its r closest neighbor can be from $\mathcal{L}_{1,0}$. \square

Next we want to prove that none of the r neighbors of $\mathbf{x} \in \mathcal{L}_{0,0}$ is in $\mathcal{L}_{1,j}, j > 0$. We show that for the case of $j = 1$, the distance property of our model suffices.

Proposition 3. *Let \mathbf{x} be a point in $\mathcal{L}_{0,0}$. Then for any $r = \mathcal{O}(1)$, none of \mathbf{x} ’s r -closest neighbors are from $\mathcal{L}_{1,1}$*

Proof. Let \mathbf{x} be any point in $\mathcal{L}_{0,0}$. Let \mathbf{x}' be \mathbf{x} ’s nearest neighbor (in Euclidean distance) from $\mathcal{L}_{1,1}$.

Let this distance be $d_{0,1}$. This implies $\min_{\mathbf{x}'' \in \mathcal{L}_{0,0}} \|\mathbf{x}' - \mathbf{x}''\| < d_{0,1}$. This implies $\min_{\mathbf{x}'' \in \mathcal{L}_{1,0}} \|\mathbf{x}' - \mathbf{x}''\| < \delta \cdot d_{0,1}$. From the second condition of Assumption 1. Then, by triangle inequality we have

$$\begin{aligned} \min_{\mathbf{x}'' \in \mathcal{L}_{1,0}} \|\mathbf{x} - \mathbf{x}''\| &\leq (1 + \delta)d_{0,1} \\ \implies (1 + \delta)d_{0,1} &\geq \frac{1}{\mu} \cdot \sup d(\mathcal{L}_{0,0}) && \text{[From Condition 1 of Assumption 1]} \\ \implies d_{0,1} &\geq \frac{1}{\mu(1 + \delta)} \sup d(\mathcal{L}_{0,0}) \\ \implies d_{0,1} &\geq \sup d(\mathcal{L}_{0,0}) \end{aligned}$$

This completes the proof. □

Next, we want to extend the proof to the further outer layers $\mathcal{L}_{1,2}, \dots, \mathcal{L}_{1,\ell}$. This is more complicated, as the data lies on some manifold, with individual layers having more complex structure. Here we use the fact that the underlying Manifold \mathcal{M} has a large reach, and get a bound on the distortion of Euclidean and Geodesic distance.

Theorem 4 (Lemma 3 of [BLW19]). *Let $S \subset \mathbb{R}^d$ be a closed set with reach τ , as defined in Definition 3. Then for any $a, b \in S$ such that $\|a - b\| < 2\tau$, one has $\frac{d_S(a,b)}{\|a-b\|} \leq \frac{2\tau}{\|a-b\|} \cdot \arcsin \frac{\|a-b\|}{2\tau}$.*

Here $\|a - b\|$ is the Euclidean distance between a, b and $d_S(\cdot, \cdot)$ is the Geodesic distance on S (for our application \mathcal{M}). We shall use this to prove that none of the r nearest neighbors of $\mathcal{L}_{0,0}$ are in \mathcal{X}_1 . Furthermore, note that $\alpha \arcsin \frac{1}{\alpha} < \pi/2$ for $\alpha > 1$.

Lemma 2. *Under the constraints of our model and $r = \mathcal{O}(1)$, if $\mu \leq (\frac{1}{c(1+\delta)})^{\ell-1}$ then none of the r -nearest Euclidean neighbor of a point in $\mathcal{L}_{0,0}$ lies in \mathcal{X}_1 . This implies that the FlowRank score of any core point is 1.*

Proof. We prove this with an induction on the minimum distance of $\mathbf{x} \in \mathcal{L}_{0,0}$ to $\mathcal{L}_{1,j}$. For any such \mathbf{x} , let $d_{0,j}$ be the minimum distance from \mathbf{x} to $\mathcal{L}_{1,j}$. In proposition 3 we have shown that $d_{0,1} \geq \frac{1}{\mu(1+\delta)} \sup d(\mathcal{L}_{0,0})$. Then, our base case is as follows.

Let $d_{0,2}$ and $\tilde{d}_{0,2}$ be the smallest distance of \mathbf{x} to $\mathcal{L}_{1,2}$ in the Euclidean and geodesic distance on \mathcal{M} , respectively. First, note that $1/c \cdot \tilde{d}_{0,2} \leq d_{0,2} \leq \tilde{d}_{0,2}$ for some $1 < c < \pi/2$. The lower bound follows from the distortion bound of Theorem 4 and the upper bound follows from the fact that geodesic distance between two points is always larger than the Euclidean distance.

Let the end points be \mathbf{y} and $\tilde{\mathbf{y}}$ respectively. Then, there exists a point $\tilde{\mathbf{x}} \in \mathcal{L}_{0,1}$ such that $d_{\mathcal{M}}(\tilde{\mathbf{x}}, \tilde{\mathbf{y}}) \leq \tilde{d}_{0,2}$. This is because, if we consider any geodesic path starting from $\mathcal{L}_{0,0}$ that goes out of \mathcal{X}_1 , it has to go through $\mathcal{L}_{0,1}, \dots, \mathcal{L}_{0,\ell}$. This is because the concentric subspaces are defined by expanding the smaller subspaces in all directions within the Manifold \mathcal{M} . Then $\|\tilde{\mathbf{x}} - \tilde{\mathbf{y}}\| \leq \tilde{d}_{0,2}$. Then, from the second condition of Assumption 1, we have

$$\min_{\mathbf{y}' \in \mathcal{L}_{1,1}} \|\mathbf{y}' - \tilde{\mathbf{y}}\| \leq \delta \cdot \tilde{d}_{0,2}$$

Let \mathbf{y}'' be the point for which the minimum is achieved. Now, we use the distances between $\mathbf{x} \in \mathcal{L}_{0,0}$, $\tilde{\mathbf{y}} \in \mathcal{L}_{1,2}$ and $\mathbf{y}'' \in \mathcal{L}_{1,1}$, we have a triangle inequality that upper bounds the minimum distance from $\mathcal{L}_{0,0}$ to $\mathcal{L}_{0,1}$, which we have defined as $d_{0,1}$ in Proposition 3. Combining, we get

$$\begin{aligned} d_{0,1} &\leq \|\mathbf{x} - \tilde{\mathbf{y}}\| + \|\tilde{\mathbf{y}} - \mathbf{y}''\| \\ \implies d_{0,1} &\leq \tilde{d}_{0,2} + \delta \cdot \tilde{d}_{0,2} \\ \implies d_{0,1} &\leq (1 + \delta)\tilde{d}_{0,2} \\ \implies \tilde{d}_{0,2} &\geq \frac{d_{0,1}}{(1 + \delta)} \\ \implies d_{0,2} &\geq \frac{d_{0,1}}{c(1 + \delta)} && \text{[From Theorem 4]} \\ \implies d_{0,2} &\geq \frac{1}{c\mu(1 + \delta)^2} \sup d(\mathcal{L}_{0,0}) \end{aligned}$$

We can continue with this inductively. Let $d_{0,j}$ is the minimum distance from $\mathbf{x} \in \mathcal{L}_{0,0}$ to $\mathcal{L}_{1,j}$. Assume $d_{0,j} \geq \frac{1}{\mu c^{j-1}(1+\delta)^j} \sup d(\mathcal{L}_{0,0})$. Note that this is proven for $d_{0,2}$.

Then, we can lower bound $d_{0,j+1}$ as follows. Consider any $\mathbf{x} \in \mathcal{L}_{0,0}$. Let $\tilde{\mathbf{y}}$ be the closest point of \mathbf{x} in $\mathcal{L}_{1,j+1}$ in geodesic distance, and the distance be $\tilde{d}_{0,j+1}$. Then, there is a point $\tilde{x} \in \mathcal{L}_{0,j}$ such that $d_{\mathcal{M}}(\tilde{x}, \tilde{\mathbf{y}}) \leq \tilde{d}_{0,j+1}$. Then $\|\tilde{x} - \tilde{\mathbf{y}}\| \leq \tilde{d}_{0,j+1}$. Then, there exists $\mathbf{y}'' \in \mathcal{L}_{1,j}$ such that $\|\mathbf{y}'' - \tilde{\mathbf{y}}\| \leq \delta \tilde{d}_{0,j+1}$. Note that this is an upper bound on $d_{0,j}$ via triangle inequality.

Then, we have

$$\begin{aligned} d_{0,j} &\leq (1 + \delta) \tilde{d}_{0,j+1} \\ \implies \tilde{d}_{0,j+1} &\geq \frac{d_{0,j}}{(1 + \delta)} \\ \implies d_{0,j+1} &\geq \frac{d_{0,j}}{c(1 + \delta)} \\ \implies d_{0,j+1} &\geq \frac{1}{\mu \cdot (c^j(1 + \delta)^{j+1})} \sup d(\mathcal{X}_{0,0}) \end{aligned}$$

This completes the induction. Then, as long as $d_{0,\ell-1} \geq \sup d(\mathcal{X}_{0,0}, \mathcal{X}_{0,0}, r)$, there are no edges from $\mathcal{L}_{0,0}$ to \mathcal{X}_1 . A trivial upper bound on $\sup d(\mathcal{L}_{0,0}, \mathcal{X}, r)$ is $\sup d(\mathcal{L}_{0,0})$ as $r = \mathcal{O}(1)$. Using this we get that if $\frac{1}{\mu c^{\ell-2}(1+\delta)^{\ell-1}} > 1$, then there are no edges going from $\mathcal{L}_{0,0}$ to \mathcal{X}_1 . This completes the proof. \square

A.3.2 Non-core points have lower score.

Next we show there exists $r = \mathcal{O}(1)$ such that for each non-core point in $\mathcal{L}_{i,j}$, one of its r nearest neighbor lies in $\mathcal{L}_{i,j-1}$. We first place some notations and results on volumes of balls on Manifolds.

Theorem 5 ([NSW08]). *Let $p \in \mathcal{M}$ which is a compact smooth m -dimensional manifold with reach τ . Consider $A = \mathcal{M} \cap B_\epsilon(p)$ where $\epsilon \ll \tau$. Then $\text{vol}(A) \geq \cos(\theta)^m \cdot \text{vol}(B_\epsilon^m(p))$ where $B_\epsilon^m(p)$ is the m -dimensional ball in T_p (the tangent space) centered at p , $\theta = \arcsin(\epsilon/2\tau)$*

Furthermore, we know that $V^m(\epsilon) = B_\epsilon^m(p)$ where we define $V^m(\epsilon)$ as the volume of the m -dimensional ball of radius ϵ . As we need a more intricate relationship between the width of the layer and the points in local neighborhood, we make some assumptions about the non-linear structure of the each of the layers.

Assumption 2.

1. We assume that all layers have the same width Δ and the reach of each sub-manifold $\mathcal{X}_{i,j}$ is $\bar{\tau}$ such that $\Delta \ll \bar{\tau} \ll \tau$. Furthermore, assume $\ell \leq m$. Furthermore, note that we do not any specific reach assumptions for the outermost layers.
2. Let there be $n_{0,0}$ points sampled in $\mathcal{L}_{0,0}$ such that $n_{0,0} = c_2 \frac{\text{Vol}(\mathcal{X}_{0,0})}{V^m(\epsilon)}$ for some $\epsilon \leq c_3 \Delta$ where $c_2 > 1$ and $c_3 < 0.001$ are constants. This, combined with Theorem 5 essentially implies that any ϵ -radius ball in $\mathcal{L}_{0,0}$ has some c_2 points on expectation.

Based on these assumptions, we have the following notion.

Proposition 4. *For any Layer $\mathcal{L}_{0,j}$. Then, the number of points $n_{0,j}$ sampled by the model satisfies $n_{0,j} \geq \frac{\text{Vol}(\mathcal{L}_{0,j})}{V^m(2\epsilon)}$*

Proof. In the definition of our model we have $\frac{n_{0,0}}{\text{Vol}(\mathcal{L}_{0,0})} = C \cdot \frac{n_{0,1}}{\text{Vol}(\mathcal{L}_{0,1})}$. Then, replacing with first condition of Assumption 2 we get

$$C \cdot \frac{n_{0,1}}{\text{Vol}(\mathcal{L}_{0,1})} \geq \frac{c_2}{V^m(\epsilon)} \implies n_{0,1} \geq \frac{c_2 \text{Vol}(\mathcal{L}_{0,1})}{C \cdot V^m(\epsilon)}$$

Continuing this for some j -steps we get $n_{0,j} \geq \frac{c_2 \text{Vol}(\mathcal{L}_{0,j})}{C^j \cdot V^m(\epsilon)}$.

However, as $C < 2$ we get $C^j V^m(\epsilon) \leq V^m(2\epsilon)$. This implies $n_{0,j} \geq \frac{c_2 \text{Vol}(\mathcal{L}_{0,j})}{V^m(2\epsilon)}$. \square

Then, we argue that for any point $\mathbf{x} \in \hat{\mathcal{L}}_{0,j}$, there exists a nearby point in $\hat{\mathcal{L}}_{0,j-1}$.

Proposition 5. *Under the constraint of Assumption 2, for any point $\mathbf{x} \in \hat{\mathcal{L}}_{0,j}$, on expectation there exists $\mathbf{x}' \in \hat{\mathcal{L}}_{0,j-1}$ such that $\|\mathbf{x} - \mathbf{x}'\| \leq 1.1\Delta$.*

Proof. This follows from our Proposition 4. Consider the closest point of \mathbf{x} in $\mathcal{L}_{0,j-1}$. Let this point be \mathbf{y}' . Consider a point $\mathbf{y}'' \in \mathcal{L}_{0,j-1}$ such that $\|\mathbf{y}' - \mathbf{y}''\| = 6\epsilon$ and the minimum distance between \mathbf{y}'' and $\mathcal{L}_{0,j'}$ for $j' \neq j-1$ is at least 4ϵ . Such a point can always be found following the definitions of the layers (which have a width of $\Delta \geq 100\epsilon$). Consider the ball $B_{3\epsilon}(\mathbf{y}'')$. Find \mathbf{y}'' such that $B_{3\epsilon}(\mathbf{y}'') \cap (\mathcal{M} \setminus \mathcal{L}_{0,j-1}) = \emptyset$. Furthermore, from Theorem 5 we have $\text{Vol}(B_{3\epsilon}(\mathbf{y}'') \cap \mathcal{M}) \geq 0.99V^m(3\epsilon)$. Then, the expected number of points in $B_{3\epsilon}(\mathbf{y}'') \cap \hat{\mathcal{L}}_{0,j-1}$ can be written as

$$\begin{aligned} \mathbb{E} \left[|\hat{\mathcal{L}}_{0,j-1} \cap \text{Vol}(B_{3\epsilon}(\mathbf{y}''))| \right] &\geq n_{0,j-1} \cdot \frac{0.99V^m(3\epsilon)}{\text{Vol}(\mathcal{L}_{0,j-1})} \\ &\geq \frac{c_2 \text{Vol}(\mathcal{L}_{0,j-1})}{V^m(2\epsilon)} \cdot \frac{V^m(3\epsilon)}{\text{Vol}(\mathcal{L}_{0,j-1})} && \text{From Proposition 4} \\ &\geq c_2 \frac{V^m(3\epsilon)}{V^m(2\epsilon)} \geq 1 \end{aligned}$$

Then, the distance of this point to \mathbf{x} is upper bounded by $\Delta + 9\epsilon \leq 1.1\Delta$.

Here the lower bound of $0.99V^m(3\epsilon)$ follows from the fact that $\cos \Theta$ in Theorem 5 gets very close to 1 when radius is much smaller than reach, which is the case here as $\epsilon \leq 0.01\Delta \ll \tau_{i,j}$. □

That is, we have proven that in our model, if you consider a radius of 1.1Δ , you can always find a neighbor in the inner layer. Then, finally, we are left to calculate what is the maximum possible points in this radius in our configuration.

Lemma 3. *Given our model and the conditions in Assumption 2, there exists $r = \mathcal{O}(1)$ such that if we consider the r -nearest neighbors of any point in $\hat{\mathcal{L}}_{0,j}$, at-least one neighbor lies in $\hat{\mathcal{L}}_{0,j-1}$. If our FlowRank algorithm is initialized with such an r , then all non-core points get a score of less than 1.*

Proof. In Proposition 5 we have obtained an upper bound on the radius that ensures this behavior. We finally calculate the maximum expected number of points in this radius. Consider the densest region of \mathcal{X}_0 , that is $\mathcal{X}_{0,0}$. Then, the number of points in a radius of 1.1Δ can be upper bounded as

$$\mathbb{E} \left[|\hat{\mathcal{X}} \cap B_{1.1\Delta}(\mathbf{x})| \right] \leq n_{0,0} \cdot \frac{\text{Vol}(B_{1.1\Delta}(\mathbf{x}))}{\text{Vol}(\mathcal{X}_{0,0})} \leq c_3 \frac{V^m(1.1\Delta)}{V^m(2\epsilon)}$$

Note that this value is exponential only in m , but as m is a constant, we get a constant upper bound on r . □

Finally, we recall the Theorem from the main paper and combine the two results we obtained formally.

Theorem (Restated Theorem 1). *Let data be generated from the LCPDM(2, ℓ) model. Assume we get the exact density of the points and expected value of randomly ascending random walk in the FlowRank algorithm. Let this be called the ideal FlowRank outcome. Then all the core points ($\hat{\mathcal{L}}_0$) get a score of 1. Additionally, all non-core points get a score < 1 .*

Proof. First we recall that $\mathcal{L}_{i,0}$ and $\mathcal{X}_{i,0}$ are synonymous. In Lemma 2 we have shown that for any point in $\mathcal{L}_{i,0}$ if the cores are sufficiently separated then all points in it (the core points) get a score of 1.

Next in Lemma 3 we show that under the additional density conditions of Assumption 2, there exists an r (that depends exponentially on the dimension of the underlying manifold \mathcal{M} , which is a constant) such that for each non-core point in $\mathcal{L}_{i,j}$, one of its r -nearest neighbor lies in $\mathcal{L}_{i,j-1}$ in expectation, and therefore the FlowRank score is less than 1. This completes our proof. □

A.4 Correctness of CoreSPECT framework given the correct layers.

Theorem (Clustering in the LCPDM model (Restated Theorem 3)). *Let X be n datapoints generated from the LCPDM($2, \ell$) model. Let us have an estimate of the density layers, given as $S_0, \dots, S_{\ell-1}$ such that $|S_j \cap \hat{\mathcal{L}}_j| = (1-f)|\hat{\mathcal{L}}_j|, j > 0$. for a sufficiently small function $f = o(1)$ that is layer preserving. Then, applying a variant of K-Means to S_0 and expanding the clustering using a CDNN graph (with correctly chosen parameters) results in clustering with $o(1)$ misclassification error rate on expectation.*

We prove this with a minimal adjustment. We have shown in Lemma 2 that all core points get a score of 1 and all non-core points get less than 1 by FlowRank. Therefore we assume $S_0 = \hat{\mathcal{L}}_0$. Furthermore, we simply set $t = 1$ for the proof. The proof is then as follows.

Proof. First from Proposition 1 we know that the log n -attempt single-round K-Means separates the core with probability $1 - o(1)$. We continue conditioned on this scenario.

Now, consider S_1 . We know $|S_1 \cap \hat{\mathcal{L}}_1| = (1-f)|\hat{\mathcal{L}}_1|$. Furthermore, as S is layer-preserving, we assume $|S_1 \cap \hat{\mathcal{L}}_3| = 0$. Otherwise, S_1 contains all points in $\hat{\mathcal{L}}_1$ and $\hat{\mathcal{L}}_2$ and we can treat them as a single-layer in our initial model definition (albeit with a more complex analysis).

Then, for all points in $\hat{\mathcal{L}}_1$, we know the following. Let $\mathbf{x} \in \hat{\mathcal{L}}_1 : \mathbf{x} \in \mathcal{X}_0$. Then $\min_{\mathbf{x}' \in \mathcal{L}_{0,0}} \|\mathbf{x} - \mathbf{x}'\| \leq \delta \cdot \min_{\mathbf{x}' \in \mathcal{L}_{1,0}} \|\mathbf{x} - \mathbf{x}'\|$. This implies if we apply our layer-expansion with one neighbor, all such points will be correctly classified.

Assume that in the worst case scenario we misclassify each $\mathbf{x} \in S_1 \cap \mathcal{M} \setminus \hat{\mathcal{L}}_1$, which is $\leq f(n)$ many points, with n being the total number of points. Lets call this set E_1 .

Then, when considering the points in S_2 , let's consider what is the criteria for this point to be correctly clustered. Consider $\mathbf{x} \in S_2 \cap \hat{\mathcal{L}}_2$. We know that on expectation there exists a point $\mathbf{x}' \in \hat{\mathcal{L}}_1$ such that $\|\mathbf{x} - \mathbf{x}'\| \leq 1.1\Delta$ (from Proposition 5). If \mathbf{x}' is either correctly classified or is present in S_1 , then \mathbf{x} is correctly clustered.

Therefore, the set of points incorrectly clustered from S_2 is upper bounded by the set of points that is within 1.1Δ distance of a misclassified point or a point in $\hat{\mathcal{L}}_1$ that is not in S_1 . Additionally, any point in S_2 that is not from $\hat{\mathcal{L}}_2$ may get incorrectly clustered.

Here, we note that the maximum number of points in the 1.1Δ -radius of any point is upper bounded by $\frac{n_{0,0}V^m(1.1\Delta)}{Vol(\mathcal{L}_{0,0})}$ assuming they are all from maximum density points. This can be simplified as

$$\frac{n_{0,0}V^m(1.1\Delta)}{Vol(\mathcal{L}_{0,0})} \leq \frac{c_2V^m(1.1\Delta)}{V^m(1.1\epsilon)} \quad [\text{From Condition 2 of Assumption 2}]$$

which we upper bound as the constant C_m (as m is fixed). Then, the total number of misclassified points in S_2 is upper bounded by

$$|E_1| \cdot C_m + |S_2 \setminus \hat{\mathcal{L}}_2| \cdot C_m + |\hat{\mathcal{L}}_1 \setminus S_1| \cdot C_m = \mathcal{O}(f(n))$$

We continue this for ℓ layers. Assume E_j points have been misclassified up to layer j . Then the number of misclassified points in S_{j+1} can be upper bounded as $|E_j| \cdot C_m + |S_{j+1} \setminus \hat{\mathcal{L}}_{j+1}| \cdot C_m + |\hat{\mathcal{L}}_j \setminus S_j| \cdot C_m$. Now, if we induct on $|E_j| = \mathcal{O}(f(n))$ then we get $|E_{j+1}| = \mathcal{O}(f(n))$. This implies that $|E_\ell| = \mathcal{O}(f(n)) = o(n)$.

This implies we finish clustering all the points with $o(n)$ many misclassifications, which leads to an $o(1)$ misclassification error rate, completing our proof. \square

Discussion of runtime. Finally, we note that given the CDNN graph, the run time of our layer-expansion method is $n \cdot k \cdot t$.

Theorem (Restated Theorem 2). *Given the CDNN graph $G_{t,S}^+$ and a clustering of S_0 , the rest of the points can be clustered in $\mathcal{O}(n \cdot k \cdot t)$ time, which is linear in the number of the edges and the number of clusters in $G_{t,S}^+$.*

Proof. All points in S_0 are already clustered. Starting with S_1 , loop through every point \mathbf{u} in S_1 and update the cluster membership vector $\hat{C}(\mathbf{u})$ and the cluster label k_u by the following: $\hat{C}(\mathbf{u}) \leftarrow \sum_{\mathbf{v} \in \mathcal{N}_{G^+}} W(\mathbf{u}, \mathbf{v}) \cdot \hat{C}(\mathbf{v}); \quad k_u \leftarrow$

$\arg \min \hat{C}(\mathbf{u})$. Repeat the same procedure with S_{j+1} once all points in S_j are clustered. Here, for each point in S_j , we look at the k -length cluster membership vector $\hat{C}(\mathbf{u})$ for some t many neighbors, which takes $\mathcal{O}(t \cdot k)$ time. This makes the total runtime $\mathcal{O}(n \cdot k \cdot t)$.

□

B Experiments

B.1 Description of datasets and experiments

As we have described, we use a total of 15 datasets in this paper. We describe the details of the datasets here. We use 11 single-cell datasets, 2 bulk-RNA datasets, and two image datasets.

Single-cell datasets: We use all of the 11 datasets from [MZ25]. The details of the datasets are as follows.

Name	# of points	# of communities	Source
Baron_Human	8569	14	[AMC ⁺ 19]
Baron_Mouse	1886	13	[AMC ⁺ 19]
Muraro	2122	9	[AMC ⁺ 19]
Segerstolpe	2133	13	[AMC ⁺ 19]
Xin	1449	4	[AMC ⁺ 19]
Zhengmix8eq	3994	8	[DRS18]
T-cell dataset	5759	10	[SVY ⁺ 18]
ALM	10068	136	[SSG ⁺ 19]
AMB	12382	110	[AMC ⁺ 19]
TM	54865	55	[AMC ⁺ 19]
VISP	15413	135	[SSG ⁺ 19]

Table 2: Details of the single-cell RNA-seq datasets

Bulk-RNA datasets: For the bulk-RNA datasets, we take patient samples from the The Cancer Genome Atlas [TCW15]. This was part of a comprehensive project launched by the ational Human Genome Research Institute (NHGRI) in 2006 to catalog genetic mutations responsible for cancer using genome sequencing and bioinformatics. The project analyzed samples of around 11,000 tumor samples across 33 cancer types (which we use as the ground-truth cluster identity). We use two modalities of datasets, mRNA and micro-RNA, which form the two bulk-RNA datasets that we use.

For the single-cell and bulk-RNA datasets, we first log-normalize it and then apply PCA dimensionality reduction of dimension $\min\{50, \# \text{ of ground truth clusters}\}$, which is a standard pipeline in the single-cell (and genomics) analysis literature [DRS18].

Image datasets: For image datasets, we use the test-set of the popular MNIST [Den12] and Fashion-MNIST [XRV17] dataset.

B.2 Comparison algorithms

Density-based clustering As we have discussed, we focus on density based and manifold based clustering. For density based clustering, we implemented HDBSCAN [CMS13]. We also implemented DBSCAN [EKS⁺96] and OPTICS [ABKS99] but were unable to use them as benchmarks, as they marked most points as outliers for most datasets. We also used three density peak clustering algorithms [RL14, WX17, YEHS23].

Manifold-based clustering For Manifold clustering, we first looked at the scikit-learn spectral clustering [VL07] implementation. We found the default setting of rbf kernel took prohibitively long time and also did not produce good quality cluster, and therefore we did not include it in our benchmarks. In comparison, the K-nearest-neighbor-based kernel had much better performance, proving to be a competent benchmark. We also implemented two recent manifold clustering algorithms [LMM20] [THL23] with theoretical guarantees but the performances were suboptimal to spectral clustering by large margins, and thus were not reported in detail in this paper. It remains as future steps to analyze the underlying cause of their ineffectiveness on real world data.

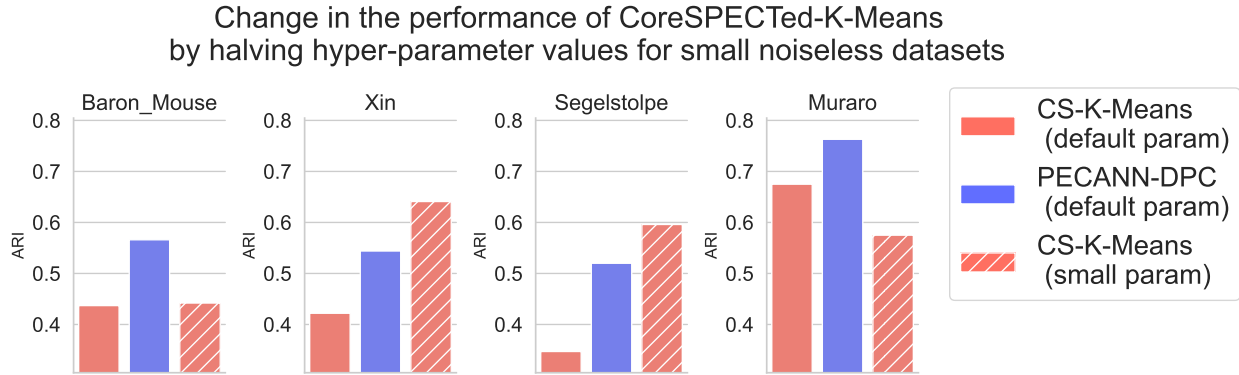


Figure 12: Enhancement in the performance of CoreSPECTed-K-Means by selecting smaller hyper-parameters for small noiseless datasets

Further comparisons Finally, we note that design of clustering algorithm is a very extensive field with new clustering algorithms being designed. Especially, both the areas of density-peak clustering and manifold clustering are very active. We aim to test our framework both on and against more such algorithms in future.

B.3 Performance of CoreSPECT on small noiseless datasets

In the main paper, we showed that for the default parameter settings CoreSPECTed-K-Means and CoreSPECTed-GMM both achieve the best rank in ARI and the second best rank in NMI. Furthermore, we noted that in the four smallest datasets (Baron Mouse, Xin, Segerstolpe, and Muraro) our performance lacked behind that of Density based clustering (especially PECANN-DPC). Here we explore this in more detail. First, we note the ARI of CoreSPECTed-K-Means and PECANN-DPC for the four datasets.

As can be observed from Table 5, PECANN-DPC has noticeably higher ARI than our method for all four datasets. First we note that all of these clusters are well-separated. This can be observed as follows. If we look at any pair of clusters, all the nearest neighbors of any point are from the same cluster. This implies, the main hurdle of “hard-to-separate-peripheral points” is not present in these datasets. However, we still want to better understand if the performance of our framework can be improved in such cases. In this direction, we observe two interrelated reasons.

1. For all of these datasets, the cores (top 10% of the points) selected by FlowRank (with default parameter) sometimes does not include any points from the smallest (such as less than 20 points) clusters.
2. In our default setting, we choose $q = 40, r = 20, t = 20$. The parameter r decides how many neighbors of a point is looked at for the ascending random walk step. If r is larger than the size of a ground truth cluster, then there is a high chance *all the points* from that cluster will have a low FlowRank value. Similarly, in our layer-expansion step, we created a t -regular CDNN graph. Even if the core has points from a small ground truth cluster that is well separated in the core-clustering step, a large t can incorrectly assign non-core points from these small clusters.

Improving on the first point falls within the overarching direction of coming up with a better core-extraction algorithm, and we believe this is a very important question. With regards to the second point, we observe that our hyper-parameters can be changed slightly to get better results on these small datasets. As an example, we run CoreSPECTed-K-means with the hyper-parameters ($q = 20, r = 10, t = 10$), that is dividing every value with 2. The comparative performance of CS-K-Means w.r.t. the changed parameters are shown in Figure 12.

As we can observe, for 2 out of 4 datasets, we have considerable improvements (more than 50%), only 2% improvement for Baron-Mouse, and the ARI value for Muraro goes down by approximately 20%. This demonstrates the potential of choosing parameters in a more principled way.

However, this comparison may seem unfair as we are only using the default parameters for PECANN. In this direction, to understand the potential of the different clustering algorithms as well as our CoreSPECT framework, we report the best clustering performance for each dataset with the best hyper-parameters chosen from a grid search. Note that we do this in a supervised manner for all the clustering algorithms. The goal of this Section is to simply present the highest accuracy that can be achieved with the method, which is more of an indicator of how well the underlying mechanisms of the algorithms relate to/fit the underlying structures of the dataset.

B.4 Exploring the potential of CoreSPECT with parameter search (and fair comparisons)

In this direction, we perform a grid search for the influential parameters of the clustering algorithms that we use for comparisons and report the best data-wise performance in ARI and NMI. The details of the parameter search procedures can be found in Section C.2. The ARI and NMI of the outcomes can be found in Tables 7 and 8 respectively.

As a summary statistics, here we present the rank of the different methods for ARI and NMI in Table 3. We observe that CoreSPECTed-K-Means achieves the highest rank in *both in NMI and ARI*. This indicates that our model formulation indeed fits the structure of real-world dataset for various domains.

	K-Means	CS-K-Means	GMM	CS-GMM	SC	PECANN-DPC	HDBSCAN	Bi-K-Means	DP	ADPclust
ARI	6.533	1.867	4.800	2.733	3.933	<u>2.667</u>	6.733	7.533	9.000	9.067
NMI	6.267	2.200	5.000	2.933	<u>2.467</u>	3.133	7.067	7.800	8.400	9.400

Table 3: Average rankings for ARI and NMI across clustering methods for dataset wise best parameter choices

	K-Means	CS-K-Means	GMM	CS-GMM	SC	PECANN-DPC	HDBSCAN	Bi-K-Means	DP	ADPclust
ARI	5.933	2.600	4.000	<u>2.933</u>	4.000	3.533	6.867	7.200	8.600	9.000
NMI	6.133	<u>2.600</u>	4.467	3.000	2.267	3.733	7.267	7.733	8.533	8.933

Table 4: Average rankings for ARI and NMI across clustering methods for default parameter choice

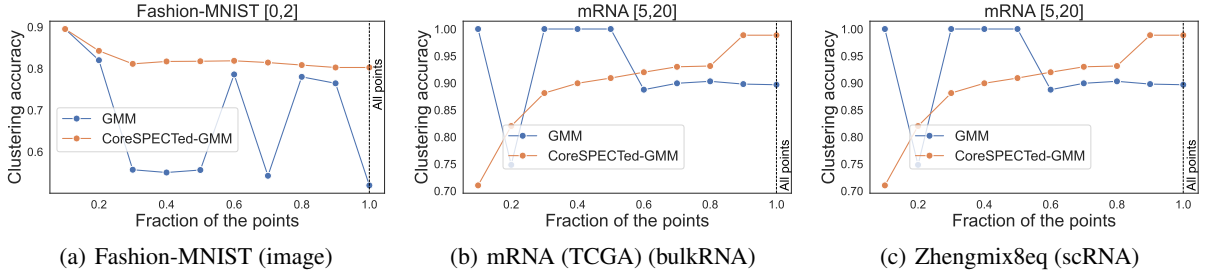


Figure 13: Comparing the accuracy of applying GMM on the top x -fraction of the points (according to FlowRank) vs. applying GMM to top 10% and then applying Layer-wise expansion up to top x -fraction, for $x \in [0.1, 0.2, \dots, 1]$ for some pairs of clusters. For $x = 0.1$ (the cores), GMM has very good performance, but as we apply GMM on the outer layers, its performance deteriorates. In contrast, the layer-wise propagation gives significantly better response, further justifying our layer-wise model and utility of our framework.

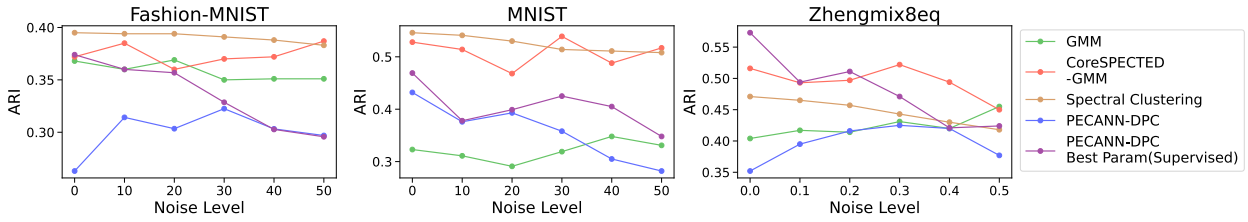


Figure 14: Comparative robustness of CoreSPECTed-GMM on datasets with Gaussian perturbation. As the noise level increases, the performance of DPC deteriorates, with CoreSPECTed-GMM demonstrating significantly higher resistance.

C Further experimental details and outcomes

C.1 CoreSPECTed GMM’s Robustness to noise and top x fraction accuracy

In addition to the figure 4 and 5 of the main paper, we also show the top x fraction accuracy of GMM and CoreSPECTed-GMM in figure 13 and the robustness to noise in figure 14. Similar to K-Means and CoreSPECTed-K-Means, it is observed that the performance of CoreSPECTed-GMM is more robust to noise and also able to achieve better clustering results as we increase the number of nodes to cluster in the order of decreasing FlowRank value.

C.2 Hyperparameter search for algorithms

For the results obtained using default hyperparameters, we have used the default hyperparameters suggested by the algorithms. Also, the true number of clusters has been passed as the hyperparameter to all the algorithms that can take it as input, which are K-Means, CoreSPECTed-K-Means, GMM, CoreSPECTed-GMM, Bisecting-K-Means, PECANN-DPC, ADPCLust, and Spectral Clustering. We have run 10 repetitions for every setting and recorded the average value and maximum absolute divergence from the average. For best hyperparameter results, we have performed grid-search over various impactful hyperparameters and reported the ones with the highest ARI value. The detailed procedure of producing the best hyperparameter result is explained below.

K-Means [Llo82], Bisecting-K-Means [KKS00], GMM [YLL12] For both default and best hyperparameter settings, only the true number of clusters was given.

CoreSPECTed-K-Means, CoreSPECTed-GMM For both default and best hyperparameter settings, the true number of clusters was given. For the best result search, we have performed grid search over three hyperparameters with the following grids: $\mathbf{q} = [10, 20, 40(\text{default})]$, $\mathbf{r} = [10, 20, 40(\text{default})]$, $\mathbf{t} = [1, 10, 20(\text{default})]$. For each dataset, the hyperparameters that yield the best ARI value in CoreSPECTed-K-Means were used for CoreSPECTed-GMM as well.

Density Peak Clustering [RL14]: The default hyperparameters are automatically calculated based on the distribution of the datapoints as shown in the paper. To further improve the performance, we have reported the best outcome of the

grid search over the main hyperparameter **density_threshold** that sets the minimum density for a datapoint to be a cluster center with the following grid: **density_threshold** = [auto, 5, 10, 15, 20]

PECANN-DPC [YEHS23]: The main hyperparameters that affect the performance of the PECANN-DPC are **K** (How many neighbors to use to estimate density) and **alpha** (how far to explore during approximate-nearest-neighbor search). For each dataset, we perform grid search to report the one with best ARI value with following grid: **K** = [6(default), 10, 20, 30, 40] and **alpha** = [1.0, 1.2(default), 1.5, 2.0]. The hyperparameter **num_clusters** is set as the true number of clusters, in order to further enhance the performance.

HDBSCAN [MHA17]: The implementation of the following source provides soft clustering that can label all the datapoints including the outliers, unlike most HDBSCAN implementations that remove outliers first. The datapoints are assigned to the cluster with highest conditional membership strengths from merge heights in the condensed tree.

As suggested by the documentation and also as empirically observed, the primary hyperparameter that affects the final clustering is **min_cluster_size**, which sets the minimum size of each cluster. We have reported the best result for each dataset with the grid search of **min_cluster_size** = [5(default), 10, 15, 20]. Even among these 4 values, the results highly varied, highlighting the high sensitivity of the hyperparameter.

ADPCLust [WX17]: The default hyperparameters are also automatically calculated according to the datapoints. To further improve the performance we have set the hyperparameter **nclust**, the number of cluster centers, as the true number of clusters. For automatic density estimation and centroid selection algorithms, the best result of all possible combinations of the algorithms were reported: **htype** = ["rot"(default), "amise"] and **ac** = [1(default), 2]

Spectral Clustering [VL07]: The **n_clusters** hyperparameter has been set as the true number of clusters. Besides that, we also performed grid search over the hyperparameter **n_neighbors** with the grid of [10, 15(default), 20, 30, 40] and reported the best value. This hyperparameter is used to set the scope of the locality of nearest neighbor edges.

C.3 Complete ARI and NMI tables

Finally, in Tables 5 and 6 we record the overall performance of all methods on all datasets. Similarly, in Tables 7 and 8 we record the performance of the methods with respect to data-wise best hyperparameters that we obtained via a grid search.

(a) Datasets 1–8

Method	mRNA	miRNA	ALM	AMB	VISP	MNIST	Fashion–MNIST	Muraro
PECANN	<u>0.722</u> ± 0.000	0.435 ± 0.000	<u>0.338</u> ± 0.000	0.384 ± 0.000	0.393 ± 0.000	0.435 ± 0.003	0.263 ± 0.000	0.763 ± 0.000
Spectral Clustering	0.589 ± 0.025	0.489 ± 0.004	0.336 ± 0.009	0.389 ± 0.032	0.341 ± 0.034	<u>0.546</u> ± 0.001	0.395 ± 0.000	0.616 ± 0.000
HDBSCAN	0.618 ± 0.000	0.578 ± 0.000	0.094 ± 0.000	0.000 ± 0.000	0.000 ± 0.000	0.409 ± 0.000	0.001 ± 0.000	0.323 ± 0.000
Bisecting -K-Means	0.539 ± 0.028	0.383 ± 0.025	0.272 ± 0.009	0.263 ± 0.010	0.226 ± 0.015	0.282 ± 0.044	0.283 ± 0.013	0.322 ± 0.015
Density Peak Clustering	0.555 ± 0.000	0.000 ± 0.000	0.000 ± 0.000	0.088 ± 0.000	0.106 ± 0.000	0.160 ± 0.000	0.239 ± 0.000	0.000 ± 0.000
ADP-Clustering	0.617 ± 0.000	0.093 ± 0.000	0.001 ± 0.000	0.005 ± 0.000	0.003 ± 0.000	0.000 ± 0.000	0.000 ± 0.000	0.006 ± 0.000
K-Means	0.595 ± 0.019	0.462 ± 0.018	0.322 ± 0.014	0.307 ± 0.021	0.274 ± 0.011	0.384 ± 0.009	0.349 ± 0.009	0.341 ± 0.002
CoreSPECTed -K-Means	0.718 ± 0.029	0.640 ± 0.019	0.416 ± 0.024	<u>0.460</u> ± 0.061	0.489 ± 0.034	0.554 ± 0.071	<u>0.380</u> ± 0.001	0.675 ± 0.003
GMM	0.672 ± 0.023	<u>0.599</u> ± 0.024	0.316 ± 0.020	0.310 ± 0.029	0.280 ± 0.005	0.319 ± 0.056	0.372 ± 0.052	<u>0.676</u> ± 0.072
CoreSPECTed -GMM	0.723 ± 0.054	0.614 ± 0.038	0.390 ± 0.029	0.462 ± 0.059	<u>0.450</u> ± 0.030	0.530 ± 0.027	<u>0.380</u> ± 0.044	0.589 ± 0.082

(b) Datasets 9–15

Method	Baron_Human	Baron_Mouse	Segerstolpe	Tcell–medicine	Zhengmix8eq	Xin	TM
PECANN	0.720 ± 0.005	0.566 ± 0.000	0.520 ± 0.000	0.081 ± 0.000	0.352 ± 0.000	0.544 ± 0.000	<u>0.588</u> ± 0.000
Spectral Clustering	0.527 ± 0.000	0.390 ± 0.000	0.348 ± 0.001	<u>0.326</u> ± 0.001	0.352 ± 0.000	0.544 ± 0.000	0.489 ± 0.013
HDBSCAN	0.024 ± 0.000	0.096 ± 0.000	0.043 ± 0.000	0.005 ± 0.000	0.000 ± 0.000	<u>0.756</u> ± 0.000	0.646 ± 0.000
Bisecting -K-Means	0.375 ± 0.044	0.239 ± 0.044	0.216 ± 0.051	0.165 ± 0.013	0.359 ± 0.076	0.430 ± 0.003	0.437 ± 0.017
Density Peak Clustering	0.000 ± 0.000	0.774 ± 0.000	OOM ± 0.000				
ADP-Clustering	0.022 ± 0.000	0.004 ± 0.000	0.000 ± 0.000	0.004 ± 0.000	0.000 ± 0.000	0.001 ± 0.000	OOM ± 0.000
K-Means	0.413 ± 0.049	0.278 ± 0.038	0.274 ± 0.036	0.201 ± 0.002	0.395 ± 0.013	0.428 ± 0.001	0.452 ± 0.033
CoreSPECTed -K-Means	<u>0.692</u> ± 0.098	<u>0.437</u> ± 0.004	0.347 ± 0.012	0.283 ± 0.016	0.518 ± 0.018	0.422 ± 0.005	0.554 ± 0.018
GMM	0.511 ± 0.046	0.306 ± 0.060	<u>0.353</u> ± 0.146	0.382 ± 0.077	0.427 ± 0.079	0.657 ± 0.180	0.514 ± 0.030
CoreSPECTed -GMM	0.566 ± 0.101	0.391 ± 0.117	0.342 ± 0.056	0.272 ± 0.021	<u>0.516</u> ± 0.034	0.450 ± 0.029	0.574 ± 0.048

Table 5: Average ARI of 10 iterations across all datasets with default hyperparameters. The maximum absolute divergence from the average is recorded with \pm

(a) Datasets 1–8

Method	mRNA	miRNA	ALM	AMB	VISP	MNIST	Fashion–MNIST	Muraro
PECANN	0.834 ± 0.000	0.718 ± 0.001	0.717 ± 0.001	0.742 ± 0.000	0.715 ± 0.001	0.570 ± 0.004	0.476 ± 0.000	<u>0.794</u> ± 0.000
Spectral Clustering	0.827 ± 0.003	0.789 ± 0.001	0.736 ± 0.007	0.765 ± 0.009	0.736 ± 0.007	<u>0.700</u> ± 0.000	0.585 ± 0.000	0.783 ± 0.000
HDBSCAN	0.809 ± 0.000	0.743 ± 0.000	0.522 ± 0.000	0.010 ± 0.000	0.007 ± 0.000	0.548 ± 0.000	0.025 ± 0.000	0.523 ± 0.000
Bisecting -K-Means	0.712 ± 0.009	0.618 ± 0.021	0.680 ± 0.006	0.699 ± 0.008	0.646 ± 0.010	0.407 ± 0.033	0.445 ± 0.019	0.501 ± 0.025
Density Peak Clustering	0.781 ± 0.000	0.000 ± 0.000	0.000 ± 0.000	0.392 ± 0.000	0.451 ± 0.000	0.489 ± 0.000	0.467 ± 0.000	0.000 ± 0.000
ADP-Clustering	0.787 ± 0.000	0.438 ± 0.000	0.054 ± 0.000	0.108 ± 0.000	0.089 ± 0.000	0.002 ± 0.000	0.003 ± 0.000	0.027 ± 0.000
K-Means	0.774 ± 0.005	0.688 ± 0.007	0.723 ± 0.004	0.740 ± 0.005	0.700 ± 0.005	0.505 ± 0.020	0.513 ± 0.021	0.521 ± 0.003
CoreSPECTed -K-Means	0.841 ± 0.007	0.810 ± 0.006	0.729 ± 0.006	0.749 ± 0.005	<u>0.733</u> ± 0.004	0.713 ± 0.020	<u>0.569</u> ± 0.001	0.799 ± 0.003
GMM	0.831 ± 0.010	0.775 ± 0.005	0.719 ± 0.005	0.739 ± 0.008	0.700 ± 0.002	0.473 ± 0.036	0.526 ± 0.014	0.689 ± 0.062
CoreSPECTed -GMM	<u>0.839</u> ± 0.009	<u>0.803</u> ± 0.010	<u>0.731</u> ± 0.005	<u>0.756</u> ± 0.006	<u>0.733</u> ± 0.001	0.690 ± 0.010	0.561 ± 0.026	0.730 ± 0.061

(b) Datasets 9-15

Method	Baron_Human	Baron_Mouse	Segerstolpe	Tcell–medicine	Zhengmix8eq	Xin	TM
PECANN	<u>0.776</u> ± 0.003	0.760 ± 0.000	0.640 ± 0.000	0.265 ± 0.001	0.625 ± 0.000	0.605 ± 0.000	0.776 ± 0.000
Spectral Clustering	0.769 ± 0.000	<u>0.692</u> ± 0.000	<u>0.633</u> ± 0.000	<u>0.464</u> ± 0.000	0.625 ± 0.000	0.605 ± 0.000	0.792 ± 0.005
HDBSCAN	0.083 ± 0.000	0.191 ± 0.000	0.160 ± 0.000	0.023 ± 0.000	0.011 ± 0.000	0.678 ± 0.000	0.775 ± 0.000
Bisecting -K-Means	0.605 ± 0.032	0.514 ± 0.036	0.442 ± 0.051	0.250 ± 0.014	0.497 ± 0.075	0.533 ± 0.013	0.679 ± 0.007
Density Peak Clustering	0.000 ± 0.000	0.767 ± 0.000	OOM				
ADP-Clustering	0.095 ± 0.000	0.030 ± 0.000	0.009 ± 0.000	0.030 ± 0.000	0.006 ± 0.000	0.007 ± 0.000	OOM
K-Means	0.636 ± 0.018	0.578 ± 0.023	0.511 ± 0.045	0.314 ± 0.002	0.561 ± 0.011	0.542 ± 0.002	0.718 ± 0.010
CoreSPECTed -K-Means	0.787 ± 0.028	0.686 ± 0.003	0.602 ± 0.008	0.394 ± 0.016	<u>0.640</u> ± 0.009	0.550 ± 0.005	0.772 ± 0.007
GMM	0.736 ± 0.012	0.610 ± 0.040	0.546 ± 0.116	0.470 ± 0.032	0.618 ± 0.033	<u>0.691</u> ± 0.082	0.784 ± 0.010
CoreSPECTed -GMM	0.757 ± 0.044	0.650 ± 0.042	0.598 ± 0.013	0.393 ± 0.012	0.660 ± 0.010	0.569 ± 0.024	<u>0.785</u> ± 0.012

Table 6: Average NMI of 10 iterations across all datasets with default hyperparameters. The maximum absolute divergence from the average is recorded with \pm

(a) Datasets 1-8

Method	mRNA	miRNA	ALM	AMB	VISP	MNIST	Fashion-MNIST	Muraro
PECANN	0.722 ± 0.000	0.607 ± 0.000	0.389 ± 0.000	0.410 ± 0.000	0.393 ± 0.000	0.469 ± 0.003	0.374 ± 0.000	0.862 ± 0.000
Spectral Clustering	0.597 ± 0.031	0.522 ± 0.003	0.357 ± 0.016	0.430 ± 0.033	0.359 ± 0.010	<u>0.563</u> ± 0.000	<u>0.399</u> ± 0.000	<u>0.690</u> ± 0.000
HDBSCAN	0.660 ± 0.000	0.578 ± 0.000	0.095 ± 0.000	0.091 ± 0.000	0.169 ± 0.000	0.426 ± 0.000	0.175 ± 0.000	0.342 ± 0.000
Bisecting -K-Means	0.539 ± 0.028	0.383 ± 0.025	0.272 ± 0.009	0.263 ± 0.010	0.226 ± 0.015	0.282 ± 0.044	0.283 ± 0.013	0.322 ± 0.015
Density Peak Clustering	0.597 ± 0.000	0.052 ± 0.000	0.008 ± 0.000	0.089 ± 0.000	0.128 ± 0.000	0.160 ± 0.000	0.239 ± 0.000	0.046 ± 0.000
ADP-Clustering	0.634 ± 0.000	0.130 ± 0.000	0.024 ± 0.000	0.021 ± 0.000	0.024 ± 0.000	0.000 ± 0.000	0.008 ± 0.000	0.027 ± 0.000
K-Means	0.595 ± 0.019	0.462 ± 0.018	0.322 ± 0.014	0.307 ± 0.021	0.274 ± 0.011	0.384 ± 0.009	0.349 ± 0.009	0.341 ± 0.002
CoreSPECTed -K-Means	0.734 ± 0.037	0.640 ± 0.019	<u>0.429</u> ± 0.034	<u>0.460</u> ± 0.061	0.489 ± 0.034	0.602 ± 0.006	0.421 ± 0.002	0.675 ± 0.003
GMM	0.672 ± 0.023	0.599 ± 0.024	0.316 ± 0.020	0.310 ± 0.029	0.280 ± 0.005	0.319 ± 0.056	0.372 ± 0.052	0.676 ± 0.072
CoreSPECTed -GMM	<u>0.723</u> ± 0.053	<u>0.614</u> ± 0.038	0.434 ± 0.017	0.462 ± 0.059	<u>0.450</u> ± 0.030	0.530 ± 0.027	0.385 ± 0.059	0.589 ± 0.082

(b) Datasets 9-15

Method	Baron_Human	Baron_Mouse	Segerstolpe	Tcell-medicine	Zhengmix8eq	Xin	TM
PECANN	0.764 ± 0.000	0.570 ± 0.001	0.550 ± 0.005	0.231 ± 0.000	0.572 ± 0.000	<u>0.823</u> ± 0.012	0.720 ± 0.016
Spectral Clustering	0.557 ± 0.000	0.427 ± 0.000	0.365 ± 0.002	<u>0.326</u> ± 0.000	0.478 ± 0.000	0.663 ± 0.000	0.508 ± 0.034
HDBSCAN	0.119 ± 0.000	0.096 ± 0.000	0.043 ± 0.000	0.005 ± 0.000	0.334 ± 0.000	0.798 ± 0.000	<u>0.646</u> ± 0.000
Bisecting -K-Means	0.375 ± 0.044	0.239 ± 0.044	0.216 ± 0.051	0.165 ± 0.013	0.359 ± 0.076	0.430 ± 0.003	0.437 ± 0.017
Density Peak Clustering	0.002 ± 0.000	0.000 ± 0.000	0.000 ± 0.000	0.002 ± 0.000	0.000 ± 0.000	0.774 ± 0.000	OOM
ADP-Clustering	0.022 ± 0.000	0.158 ± 0.000	0.044 ± 0.000	0.004 ± 0.000	0.005 ± 0.000	0.001 ± 0.000	OOM
K-Means	0.413 ± 0.049	0.278 ± 0.038	0.274 ± 0.036	0.201 ± 0.002	0.395 ± 0.013	0.428 ± 0.001	0.452 ± 0.033
CoreSPECTed -K-Means	<u>0.729</u> ± 0.082	<u>0.437</u> ± 0.004	0.628 ± 0.011	0.284 ± 0.014	0.585 ± 0.011	0.881 ± 0.008	0.569 ± 0.031
GMM	0.511 ± 0.046	0.306 ± 0.060	0.353 ± 0.146	0.382 ± 0.077	0.427 ± 0.079	0.657 ± 0.180	0.514 ± 0.030
CoreSPECTed -GMM	0.625 ± 0.133	0.391 ± 0.117	<u>0.555</u> ± 0.190	0.286 ± 0.035	<u>0.576</u> ± 0.029	0.784 ± 0.160	0.588 ± 0.039

Table 7: Average ARI of 10 iterations across all datasets with best hyperparameters. The maximum absolute divergence from the average is recorded with \pm

(a) Datasets 1-8

Method	mRNA	miRNA	ALM	AMB	VISP	MNIST	Fashion-MNIST	Muraro
PECANN	0.834 ± 0.000	0.794 ± 0.000	0.711 ± 0.001	0.742 ± 0.001	0.715 ± 0.001	0.588 ± 0.003	0.567 ± 0.000	0.831 ± 0.000
Spectral Clustering	0.829 ± 0.006	0.802 ± 0.001	<u>0.740</u> ± 0.005	0.771 ± 0.008	0.737 ± 0.005	<u>0.712</u> ± 0.000	0.589 ± 0.000	<u>0.816</u> ± 0.000
HDBSCAN	0.820 ± 0.000	0.743 ± 0.000	0.513 ± 0.000	0.408 ± 0.000	0.583 ± 0.000	0.482 ± 0.000	0.339 ± 0.000	0.564 ± 0.000
Bisecting -K-Means	0.712 ± 0.009	0.618 ± 0.021	0.680 ± 0.006	0.699 ± 0.008	0.646 ± 0.010	0.407 ± 0.033	0.445 ± 0.019	0.501 ± 0.025
Density Peak Clustering	0.802 ± 0.000	0.432 ± 0.000	0.145 ± 0.000	0.399 ± 0.000	0.517 ± 0.000	0.489 ± 0.000	0.467 ± 0.000	0.156 ± 0.000
ADP-Clustering	0.785 ± 0.000	0.370 ± 0.000	0.167 ± 0.000	0.201 ± 0.000	0.225 ± 0.000	0.002 ± 0.000	0.045 ± 0.000	0.063 ± 0.000
K-Means	0.774 ± 0.005	0.688 ± 0.007	0.723 ± 0.004	0.740 ± 0.005	0.700 ± 0.005	0.505 ± 0.020	0.513 ± 0.021	0.521 ± 0.003
CoreSPECTed -K-Means	<u>0.845</u> ± 0.008	0.810 ± 0.006	<u>0.740</u> ± 0.006	0.749 ± 0.005	<u>0.733</u> ± 0.004	0.717 ± 0.004	<u>0.587</u> ± 0.002	0.799 ± 0.003
GMM	0.831 ± 0.010	0.775 ± 0.005	0.719 ± 0.005	0.739 ± 0.008	0.700 ± 0.002	0.473 ± 0.036	0.526 ± 0.014	0.689 ± 0.062
CoreSPECTed -GMM	0.846 ± 0.009	<u>0.803</u> ± 0.010	0.743 ± 0.006	<u>0.756</u> ± 0.006	<u>0.733</u> ± 0.001	0.654 ± 0.026	0.565 ± 0.031	0.730 ± 0.061

(b) Datasets 9-15

Method	Baron_Human	Baron_Mouse	Segerstolpe	Tcell-medicine	Zhengmix8eq	Xin	TM
PECANN	0.799 ± 0.000	0.765 ± 0.002	0.650 ± 0.004	0.316 ± 0.000	<u>0.685</u> ± 0.000	<u>0.769</u> ± 0.011	0.813 ± 0.006
Spectral Clustering	0.790 ± 0.000	<u>0.718</u> ± 0.000	0.651 ± 0.001	<u>0.464</u> ± 0.000	0.671 ± 0.000	0.733 ± 0.000	<u>0.796</u> ± 0.005
HDBSCAN	0.286 ± 0.000	0.191 ± 0.000	0.160 ± 0.000	0.023 ± 0.000	0.637 ± 0.000	0.755 ± 0.000	0.775 ± 0.000
Bisecting -K-Means	0.605 ± 0.032	0.514 ± 0.036	0.442 ± 0.051	0.250 ± 0.014	0.497 ± 0.075	0.533 ± 0.013	0.679 ± 0.007
Density Peak Clustering	0.012 ± 0.000	0.000 ± 0.000	0.000 ± 0.000	0.071 ± 0.000	0.000 ± 0.000	0.767 ± 0.000	OOM
ADP-Clustering	0.095 ± 0.000	0.113 ± 0.000	0.035 ± 0.000	0.030 ± 0.000	0.016 ± 0.000	0.007 ± 0.000	OOM
K-Means	0.636 ± 0.018	0.578 ± 0.023	0.511 ± 0.045	0.314 ± 0.002	0.561 ± 0.010	0.542 ± 0.002	0.718 ± 0.010
CoreSPECTed -K-Means	<u>0.791</u> ± 0.020	0.686 ± 0.003	0.713 ± 0.007	0.398 ± 0.013	0.704 ± 0.012	0.818 ± 0.009	0.775 ± 0.009
GMM	0.736 ± 0.012	0.610 ± 0.040	0.546 ± 0.116	0.470 ± 0.034	0.618 ± 0.033	0.691 ± 0.082	0.784 ± 0.010
CoreSPECTed -GMM	0.759 ± 0.048	0.650 ± 0.042	<u>0.671</u> ± 0.083	0.404 ± 0.011	0.682 ± 0.029	0.719 ± 0.117	0.788 ± 0.014

Table 8: Average NMI of 10 iterations across all datasets with best hyperparameters. The maximum absolute divergence from the average is recorded with \pm

(a) Datasets 1–8

Method	mRNA	miRNA	ALM	AMB	VISP	MNIST	Fashion MNIST	Muraro
PECANN	K=6, alpha=1.2	K=40, alpha=1.0	K=40, alpha=1.0	K=6, alpha=1.0	K=6, alpha=1.2	K=40, alpha=1.0	K=30, alpha=1.0	K=20, alpha=1.0
Spectral Clustering	n_nbr =20	n_nbr =10	n_nbr =10	n_nbr =10	n_nbr =10	n_nbr =10	n_nbr =10	n_nbr =10
HDBSCAN	min_clust _size=20	min_clust _size=5	min_clust _size=20	min_clust _size=15	min_clust _size=15	min_clust _size=10	min_clust _size=20	min_clust _size=10
Bisecting -K-Means	default	default	default	default	default	default	default	default
Density Peak Clustering	density _thr=5	density _thr=5	density _thr=5	density _thr=5	density _thr=5	default	default	density _thr=5
ADP -Clustering	ac:1, htype:amise	ac:2, htype:rot	ac:2, htype:rot	ac:2, htype:rot	ac:2, htype:rot	ac:1, htype:rot	ac:2, htype:rot	ac:2, htype:rot
K-Means	default	default	default	default	default	default	default	default
CoreSPECTed -K-Means	q, r, t= [40, 30, 20]	q, r, t= [40, 20, 20]	q, r, t= [20, 20, 20]	q, r, t= [40, 20, 20]	q, r, t= [40, 20, 20]	q, r, t= [40, 40, 1]	q, r, t= [40, 40, 1]	q, r, t= [40, 20, 20]
GMM	default	default	default	default	default	default	default	default
CoreSPECTed -GMM	q, r, t= [40, 30, 20]	q, r, t= [40, 20, 20]	q, r, t= [20, 20, 20]	q, r, t= [40, 20, 20]	q, r, t= [40, 20, 20]	q, r, t= [40, 40, 1]	q, r, t= [40, 40, 1]	q, r, t= [40, 20, 20]

(b) Datasets 9–15

Method	Baron_Human	Baron_Mouse	Segerstolpe	Tcell–medicine	Zhengmix8eq	Xin	TM
PECANN	K=40, alpha=1.0	K=6, alpha=1.5	K=6, alpha=1.0	K=40, alpha=1.0	K=20, alpha=1.0	K=10, alpha=1.0	K=20, alpha=1.0
Spectral Clustering	n_nbr =10	n_nbr =10	n_nbr =10	n_nbr =15	n_nbr =10	n_nbr =20	n_nbr =10
HDBSCAN	min_clust _size=15	min_clust _size=5	min_clust _size=5	min_clust _size=5	min_clust _size=15	min_clust _size=20	min_clust _size=5
Bisecting -K-Means	default	default	default	default	default	default	default
Density Peak Clustering	density _thr=5	default	default	density _thr=5	default	default	OOM
ADP -Clustering	ac:1, htype:rot	ac:2, htype:rot	ac:2, htype:rot	ac:1, htype:rot	ac:2, htype:rot	ac:1, htype:rot	OOM
K-Means	default	default	default	default	default	default	default
CoreSPECTed -K-Means	q, r, t= [50, 10, 10]	q, r, t= [40, 20, 20]	q, r, t= [20, 20, 10]	q, r, t= [40, 20, 10]	q, r, t= [40, 10, 1]	q, r, t= [10, 10, 10]	q, r, t= [40, 20, 20]
GMM	default	default	default	default	default	default	default
CoreSPECTed -GMM	q, r, t= [50, 10, 10]	q, r, t= [40, 20, 20]	q, r, t= [20, 20, 10]	q, r, t= [40, 20, 10]	q, r, t= [40, 10, 1]	q, r, t= [10, 10, 10]	q, r, t= [40, 20, 20]

Table 9: Best hyperparameters found for every method. The true number of clusters was also given as input hyperparameter to the following methods: K-Means, CoreSPECTed-K-Means, GMM, CoreSPECTed-GMM, Bisecting-K-Means, PECANN-DPC, ADPCLust, and Spectral Clustering